NAVAL POSTGRADUATE SCHOOL
Monterey , California

THESIS

FLOW VISUALIZATION OF THE AIRWAKE
OF AN OSCILLATING
GENERIC SHIP MODEL

by

John L. Biskaduros

December 1987

Thesis Advisor   J. Val. Healey

REPORT DOCUMENTATION PAGE

1a. REPORT SECURITY CLASSIFICATION UNCLASSIFIED		1b. RESTRICTIVE MARKINGS			
2a. SECURITY CLASSIFICATION AUTHORITY -		3. DISTRIBUTION/AVAILABILITY OF REPORT Approved for public release; distribution is unlimited.			
2b. DECLASSIFICATION/DOWNGRADING SCHEDULE					
4. PERFORMING ORGANIZATION REPORT NUMBER(S)		5. MONITORING ORGANIZATION REPORT NUMBER(S)			
6a. NAME OF PERFORMING ORGANIZATION Naval Postgraduate School	6b. OFFICE SYMBOL (If applicable) 67	7a. NAME OF MONITORING ORGANIZATION Naval Postgraduate School			
6c. ADDRESS (City, State, and ZIP Code) Monterey, California 93943-5000		7b. ADDRESS (City, State, and ZIP Code) Monterey, California 93943-5000			
8a. NAME OF FUNDING/SPONSORING ORGANIZATION	8b. OFFICE SYMBOL (If applicable)	9. PROCUREMENT INSTRUMENT IDENTIFICATION NUMBER			
8c. ADDRESS (City, State, and ZIP Code)		10. SOURCE OF FUNDING NUMBERS			
		PROGRAM ELEMENT NO.	PROJECT NO.	TASK NO	WORK UNIT ACCESSION NO.

11. TITLE (Include Security Classification) Flow Visualization of the Airwake of an Oscillating Generic Ship Model

12. PERSONAL AUTHOR(S)
Biskaduros, John L.

13a. TYPE OF REPORT Master's Thesis	13b. TIME COVERED FROM _____ TO _____	14. DATE OF REPORT (Year, Month, Day) 1987 Dec .	15. PAGE COUNT 53

16. SUPPLEMENTARY NOTATION

17	COSATI CODES		18. SUBJECT TERMS (Continue on reverse if necessary and identify by block number)
FIELD	GROUP	SUB-GROUP	Flow Visualization, ABL, Oscillating Mechanism, Ship Motion, Aerosol, Helium Bubbles

19. ABSTRACT (Continue on reverse if necessary and identify by block number)

An experimental flow visualization study was done on an oscillating generic ship model in the Low Speed Wind Tunnel Facility at the Naval Postgraduate School in Monterey, California. The purpose was to visually analyze the flowfield around the model while simulating ship motion in rough seas, with a correspondingly modelled open-ocean atmospheric boundary layer.

The two flow visualization techniques utilized were neutral density helium bubbles and a liquid aerosol, each technique providing varying degrees of on-body and off-body analysis. Limited success was achieved with the aerosol, but the helium bubbles produced excellent photographic results and an accurate visualization of the oscillating model's flow field was achieved.

20. DISTRIBUTION/AVAILABILITY OF ABSTRACT ☒ UNCLASSIFIED/UNLIMITED ☐ SAME AS RPT ☐ DTIC USERS	21. ABSTRACT SECURITY CLASSIFICATION unclassified	
22a. NAME OF RESPONSIBLE INDIVIDUAL Healey, J. Val	22b. TELEPHONE (Include Area Code) (408)646-2804	22c. OFFICE SYMBOL 67He

DD FORM 1473, 84 MAR

83 APR edition may be used until exhausted.
All other editions are obsolete

SECURITY CLASSIFICATION OF THIS PAGE

☆ U.S. Government Printing Office: 1986—606-24.

1

Flow Visualization of the Airwake
of an Oscillating
Generic Ship Model

by

John L. Biskaduros
Lieutenant, United States Navy
B.S., Marquette University, 1979

Submitted in partial fulfillment of the
requirements for the degree of

MASTER OF SCIENCE IN AERONAUTICAL ENGINEERING

from the

NAVAL POSTGRADUATE SCHOOL
December 1987

ABSTRACT

An experimental flow visualization study was done on an oscillating generic ship model in the Low Speed Wind Tunnel Facility at the Naval Postgraduate School in Monterey, California. The purpose was to visually analyze the flowfield around the model while simulating ship motion in rough seas, with a correspondingly modelled open-ocean atmospheric boundary layer.

The two flow visualization techniques utilized were neutral density helium bubbles and a liquid aerosol, each technique providing varying degrees of on-body and off-body analysis. Limited success was achieved with the aerosol, but the helium bubbles produced excellent photographic results and an accurate visualization of the oscillating model's flow field was achieved.

TABLE OF CONTENTS

LIST OF TABLES

LIST OF FIGURES

ACKNOWLEDGEMENTS

I. INTRODUCTION

Helicopter flight operations aboard U. S. Navy combatants and auxiliary ships have become an important aspect of present fleet readiness. These operations can become quite hazardous, particularly in the takeoff and landing phases when combined with excessive ship motion and superstructure airwake turbulence. The Naval Air Test Center (NATC) presently determines the safe operating envelopes for various ship-helicopter combinations, and according to Carico, McCallum, and Higman [Ref. 1] there is a backlog involving eleven different helicopters and twenty classes of ships. At this time, disregarding the inevitable development of new ships and helicopters, it is estimated that all the safe operating envelope combinations cannot be determined within the remainder of this century. Thus, it is highly desireable to develop a simulation technique accurately establishing these safe envelopes, which would save time, costs (now at $75,000 to $150,000 per combination), and require no operational assets.

This report is concerned with the analysis of the ship airwake turbulence of an oscillating model by flow visualization with respect to the above problem. Two flow visualization techniques were attempted to accomplish this: neutral density helium bubbles and an aerosol spray, each of which provided various levels of insight towards the flowfield. Each method also required different photographic and lighting procedures to achieve optimum results. Experimentation was conducted in the Naval Postgraduate School's low speed wind tunnel modified to simulate an open-ocean atmospheric boundary layer velocity profile and associated low altitude turbulence levels. An oscillating mechanism was designed and modified by Prof. J. V. Healey, and was used to approximate ship motion in relatively rough seas. The ship model used was a generic destroyer constructed of a medium-density polystyrene foam body with an aluminum bow, scaled approximately at 170:1 to a Spruance-class destroyer. Both on-body and off-body flows were investigated by the flow visualization techniques listed above. Flows were investigated initially in the single degree-of-freedom modes of roll and pitch, then were analyzed in combinations of the above to possibly determine any non-linear coupled affects.

9

This report deals with a portion of an ongoing investigation. Preceding research included verification of the atmospheric boundary layer modelled in the wind tunnel, as well as evaluation of a similar generic model in static conditions only, using various flow visualization techniques. It is intended that further study will analyze the flows about specific ship types, using highly detailed models (some of these include the Spruance-class destroyer, Enterprise-class carrier, and New Jersey-class battleship). The final phase of research anticipates the inclusion of specific helicopter simulators to study the interactions of the two bodies in the dynamic open-air ocean environment.

Photographic results are included and discussed in the final chapter, as well as recommendations for the follow-on phases of the project.

II. ATMOSPHERIC BOUNDARY LAYER SIMULATION

A. THEORETICAL CONSIDERATIONS

Numerous studies have indicated that the turbulent boundary layer simulation based solely on the mean velocity profile is insufficient. According to Healey [Ref. 2: p. 46], there are four important parameters which must be considered:

1. The mean longitudinal windspeed, U, which is the instantaneous windspeed averaged over a specific length of time.

2. The standard deviation, σ, of the windspeed fluctuations about the mean which yields the "turbulence intensity" when divided by the mean windspeed.

3. The longitudinal scale length of the turbulence, L, a measure of the mean length of the most energetic eddies in the turbulence.

4. The spectrum function of the turbulence, an indication of the frequency distributions of the turbulence energy.

These four parameters have been empirically shown to be functions of the mean windspeed, the elevation in the boundary layer, and the roughness length scale, the latter being a surface irregularity coefficient not directly related to ground obstacle height. The roughness scale is designated as z_0, measured in meters, and ranges from 10^{-5} meters for a glassy surface to 3-4 meters for very rough-textured terrains. A more detailed listing for various types of terrain is available in [Ref. 3]

Garratt [Ref. 4] approximates the roughness length z_0 as

$$10 \exp \{-0.41 \ (0.75 + 0.067 \ x \ U(10))^{1 \ 2} \ x \ 10E\text{-}3\} \hspace{2cm} \text{(eqn 2.1)}$$

where .41 is the Von Karman constant, the square root value represents the neutral drag coefficient, and U(10) designates the mean windspeed at a 10 meter altitude. Keep in mind that this is a general approximation, since several parameters may be lost due to experimental scatter. The 10 meter elevation figure is used in the equation because this is a standard reference height often used by meteorologists, and it also coincides with the mean height for the helicopter landing decks of modern frigates and destroyers.

Recent experimentation has revealed that the turbulence intensity has some dependence on the mean windspeed, but the effect is small enough that it will be

neglected here. More importantly, it is the fluctuations in the longitudinal velocity component that determine the turbulence. The two major physical parameters influencing these velocity fluctuations are the altitude and roughness length scale. As discussed above, the altitude will be considered constant at 10 meters and a mean windspeed of 25 m sec (about 50 kts) is indicative of "normal" operating conditions in heavier seas.

Using the mean windspeed value of 25 m sec in equation 2.1, z_0 is found to be .0024 meters. Comparing to other sources [Refs. 3,5], the turbulence intensity is calculated to be 0.14. The term "rough seas" here is used in the same context as that defined by Kent [Ref. 6: p. 22], with a mean wave height of 14 feet. For this condition (sea state 5), the roughness length will be considered to range from .001 to .01 and the corresponding turbulence intensity range to be 0.13 to 0.17. Recall from earlier, the turbulence intensity is the standard deviation of the fluctuations divided by the mean wind speed.

More important than the longitudinal turbulence length scale parameter is the ratio of this length scale to the ship's beam. As this ratio increases, the actual flowfield about the ship appears to be less random and more time-dependent.

Several spectrum function models are currently available to describe the atmospheric turbulence, such as those by Kaimal, Dryden, and Von Karman. The Von Karman function is more popular and is given by

$$S(n) = (4L\sigma) / U\{1 + 70.8(n')^2\}^{5/6} \qquad \text{(eqn 2.2)}$$

where $S(n)$ is the value of the Von Karman spectrum function, n' is defined as Ln/U, L is the turbulence length scale, U is the longitudinal mean velocity, and n is the turbulence frequency.

B.   EXPERIMENTAL SIMULATION

Numerous approaches have been developed in atmospheric boundary-layer simulation (or ABL), but few take into account all four of the parameters listed previously. The best source of information available in this area has been found to be the Journal of Wind Engineering and Industrial Aerodynamics. One major difficulty in simulating an accurate over-ocean ABL is in the comparison with experimentally recorded data, since the ABL is different for changes in wind velocity, sea state, and meteorological conditions.

Also, the source of data being compared must be examined. NATC data is generally obtained using ship anemometers as the primary source of windspeed measurement. These devices measure only the relative windspeed (between the actual windspeed and the ship's speed), and as stated earlier, the atmospheric boundary layer changes only with respect to the true windspeed. Of less importance, but a justifiable consideration of error source, is that NATC tests have shown anemometer positioning in ship superstructures is susceptible to airwake interference and therefore the reliability of the instruments themselves is questionable. They are normally calibrated to avoid this, but meteorologists would not use them in a data collection study.

In dealing with ship motion relative to the ABL, scaling factors must be utilized to truly model the combined airwake in the wind tunnel. It is here the Strouhal number is introduced. This is a dimensionless quantity defined by the frequency of motion oscillation, n, multiplied by the characteristic length, L, (in this case, the ship's beam is used) divided by the speed, U, as given in the following equation:

$$\text{Strouhal Number} = n \times L / U \qquad \text{(eqn 2.3)}$$

While n, L, and U may vary from the actual system to the wind tunnel model, their ratios, defined by Strouhal numbers, must be equal for accurate modelling. Typically, as was the case in this situation, the model characteristic length is fixed by the size of the test section, and U may often be limited by the minimum Reynolds number needed and by the power capabilities of the motor driving the fan. This leaves the model oscillation frequency as the primary variable and thus is easily determined. The calculations used for the Strouhal Numbers are tabulated in the following chapter in Table I.

In view of the above, the most successful technique encountered in developing a reliable ABL wind tunnel model was presented by Counihan [Ref. 7]. He utilized vortex generators well forward of the test section to create the appropriate mean windspeed profile. Following the vortex generators were roughness elements, mounted low to the wind tunnel floor, to provide the necessary low-level turbulence. The mean speed profile, as described by Arya [Ref. 8], is the well known logarithmic relationship

$$U / U' = (1 / K) \ln (Z / z_0) \qquad \text{(eqn 2.4)}$$

where U' is the frictional velocity, K is Von Karman's constant (previously used in 2.1 as 0.41), z is the elevation and z_0 is the roughness parameter (.001 to .01, as previously determined). This expression may be refined into an exponential form as

$$U / U' = (Z / Z_g)^{1.9} \qquad \text{(eqn 2.5)}$$

where now the roughness parameter becomes the gradient height, Z_g, in this form. For the selected mean speed of 25 m/sec at 10 meters elevation for this experiment, the mean velocity profile in 2.5 becomes

$$U = 25 \times (Z / 10)^{1.9} \qquad \text{(eqn 2.6)}$$

Through the correct combination and placement of the vortex generators and the roughness elements, the above velocity profile with verified turbulence intensities (representing the atmospheric shear stresses) was obtained in the Naval Postgraduate School's low-speed wind tunnel [Ref. 9: pp. 21-28].

III. SHIP MOTION

A. THEORETICAL CONSIDERATIONS

Actual ship motion is a complex, non-linear system with six degrees of freedom (or DOF). The system may be approximated by the sixth-order equation of the following mass-damper system:

$$M\,Y''(t) + D\,Y'(t) + K\,Y(t) = F(t) \qquad \text{(eqn 3.1)}$$

where M, D, and K are six-by-six matrices and F and Y are six-dimensional vectors of $(x,y,z,\varphi,\theta,\psi)$. It is noted that F(t) may be random or sinusoidal forcing functions in the form of forces or moments. (x,y,z) represent the three translational modes of surge, sway, and heave (respectively), while (φ,θ,ψ) describe the roll, pitch, and yaw rotational modes. The system is made more complex in that coupling between modes occurs; normally roll, sway and yaw are coupled together as are heave, pitch and surge. Finally, ship interaction with the immediately surrounding water and wave action affects the mass (M), damping (D), and restoring (K) matrices so that the final system requires very large-scale computation and numerical approximation methods. Perhaps the most difficult calculation is referred to as the "encounter frequency." This is a function of the ship's natural motion frequencies (one in each DOF) and the frequencies of the ocean waves, each having their own spectrum functions; it also has a strong dependence on the angle between the ship's heading and the dominant wave direction.

Two distinct methods currently prevail in ship motion prediction programs. The more classical time-domain approach calculates (or approximates) the coefficient matrices, and often utilizes coordinate transformations to decouple certain modes for more simple analyses. These are often required to use small-angle approximation theory and thus the accuracy falls off as higher amplitudes of motion are encountered. The frequency analysis method correlates the energies of the encounter wave to the ship's response, the resultant scaling factor referred to as the Response Amplitude Operator, or RAO. Determination of these operators is relatively simple, but a huge number is required since the RAO changes with ship's heading and speed, sea condition, wave frequency, and each DOF.

15

Healey [Ref. 2: p. 52] lists three ship-motion programs in use, the one from David Taylor Naval Ship Research and Developement Center (DTNSRDC) being the most sophisticated. The following assumptions are applicable:

- Monohull ship form (entails all present U.S. Naval Ships)
- Strip theory (a common aerodynamic technique analyzing the ship's transverse sections in two dimensional flow)
- Linearized equations are valid (an update to the program accounts for non-linear roll effects)
- The RAO's are derivable from wave and ship motion harmonics
- Heave, pitch, and surge are uncoupled from roll, sway and yaw.

This is a relatively effective ship motion program, but adjustments must be made as more information in this field becomes available, particularly in the area of non-linear angular motion. It is also imperative that this, as with any simulation techniques, be validated as soon as time permits against the actual ships which are being modelled.

B. EXPERIMENTAL SIMULATION

It is the intent of this phase of the project to establish an oscillating mechanism for a generic ship model, thus several approximations and assumptions were made initially. Primary emphasis was on the individual analysis of the major modes of heave, pitch, and roll and any interactions between those. This is supported by Kent [Ref. 6: p. 41], in which he states each of the six motions are analyzed only one at a time, then the attempt is made to trace the effects of each mode on all the others. Due to fluid resistance forces, even for a ship in calm waters, any movement in any one mode will cause a response in the ship in all five other modes. Simplifying assumptions were made for each mode, such as the following for the pitching mode [Ref. 6: pp. 75-76]:

(1) The swell consists of a regular series of waves, uniform in dimension and sinusoidal in shape
(2) The "encounter angle" is zero degrees (or head-on) at constant speed
(3) Pitching is isochronous
(4) Pitch damping from water resistance is neglected
(5) Ship wake and ocean wave interference is neglected
(6) Variations in virtual mass and effects from ship's rise or fall is ignored.

The other primary objective at this stage is to optimize the flow visualization and photographic techniques for this oscillating, bluff body-type flow. With these goals in mind, an extensive ship's motion program as described previously is not required at this time, since a more basic understanding of the aerodynamics involved is being sought. This provides for a simple ships' motion model indeed, but much more research is required before accurate ship motion programs can be extensively applied to wind tunnel testing.

As discussed earlier on page 13, rotational speeds were determined by equating the Strouhal Numbers, shown by equation 2.3, for the ship and the generic model. The simulated conditions previously listed are summarized here in Table 1, as well as the parameters used in the wind tunnel. (Ship characteristic length and roll rates were obtained from personal conversation with Mr. J. Higman of NATC).

<div style="border:1px solid black; padding:1em;">

TABLE 1
FREQUENCIES OF MOTION

	SHIP	MODEL
L_{beam}	17 meters	0.1 meter
Velocity	25 m/sec	2.0 m/sec
Roll Rate	10-15 sec/cycle	
equates to	0.067-0.1 Hz	yields 0.9-1.4 Hz
Pitch Rate	7-10 sec/cycle	
equates to	0.1-0.14 Hz	yields 1.4-1.9 Hz

</div>

Bluff bodies, as referred to above, are defined as non-streamlined bodies generating separated flow over a substantial proportion of their surface. These bodies are often characterized by sharp leading-edged geometric shapes of wide angles. Until

recently little concern has been shown in their relation to the surrounding flowfields. This area of study is now referred to as "bluff body aerodynamics," and the primary interests lies in the fields of architecture and automotive engineering. The model used during this testing may be considered similar to a long, low building, thus those governing principles may be applied to the project. Unfortunately, for anything other than a basic geometric shape like a cylinder or a rectangle, little has been accomplished in this area with respect to detailed analytical testing. Bearman has done extensive study on an oscillating cylinder, but concedes that more work must be done. [Ref. 10: pp. 195-219].

Two phenomena particularly interesting with oscillating bluff bodies is the generation of trailing vortices and flow detachment. It would be advantageous in certain situations, such as a helicopter landing on a ship, to have information like the amplitudes of the trailing vortices, areas more prone to detaching flows and therefore more turbulent flow, and how these areas and their frequencies of occurrence are affected by bluff body oscillations, for some examples.

IV. EXPERIMENTAL APPARATUS

A.   WIND TUNNEL FACILITIES

The low-speed smoke tunnel located at the Naval Postgraduate School in Monterey, California, was used for all experimentation. It consists of a 15 square foot intake section with a honeycomb screen combination to prevent debris ingestion and provide some directionality to the inbound flow and reducing the turbulence in the test section. A square bell-type contraction cone leads to a 5 square foot, 22-foot long closed test section, partially enclosed by plexiglass sheets in the walls and ceiling for observation and photography. A constant-speed, AC-motor is used to drive a variable pitch 5-foot diameter fan which is preceeded by protection louvres, located directly behind the test section. The sixteen-blade fan is capable of producing speeds from virtually 0 to approximately 35-feet per second. The tunnel exit section is then routed to the environment for exhaust.

Several modifications were required to obtain a proper ABL simulation. The scheme suggested by Counihan (et al) was implemented in the following manner: vortex generators, to slow the lower-level flow and create the desired velocity profile, were constructed and installed at the leading edge of the tunnel. Four were found to be sufficient in producing the profile (as per verification measurements described in the following section), but spaces between each were wide enough to allow "tubes" of unaffected flow, which required the addition of the three tapered delay cones. The desired turbulence intensity was then obtained by using three-eighth inch dowels ranging from 2 to 8 inches in height as the roughness elements. Equally spaced one inch blocks were attempted earlier with poor results. The dowels were randomly placed and the turbulence intensity was measured, then several iterations were required before the desired intensity level, as described in Chapter II, was achieved. (Fig. 4.1).

B.   VERIFICATION OF RESULTS

Bolinger [Ref. 9: pp. 20-25] completely describes the verification procedures and methods, which are summarized here. Measurements were obtained from two different instruments to ensure accurate data was taken: first by an EDM-2500C micromanometer and then by a Dantec hotwire anemometer attached to a single wire probe. One hundred forty-four data positions were measured in the test section area,
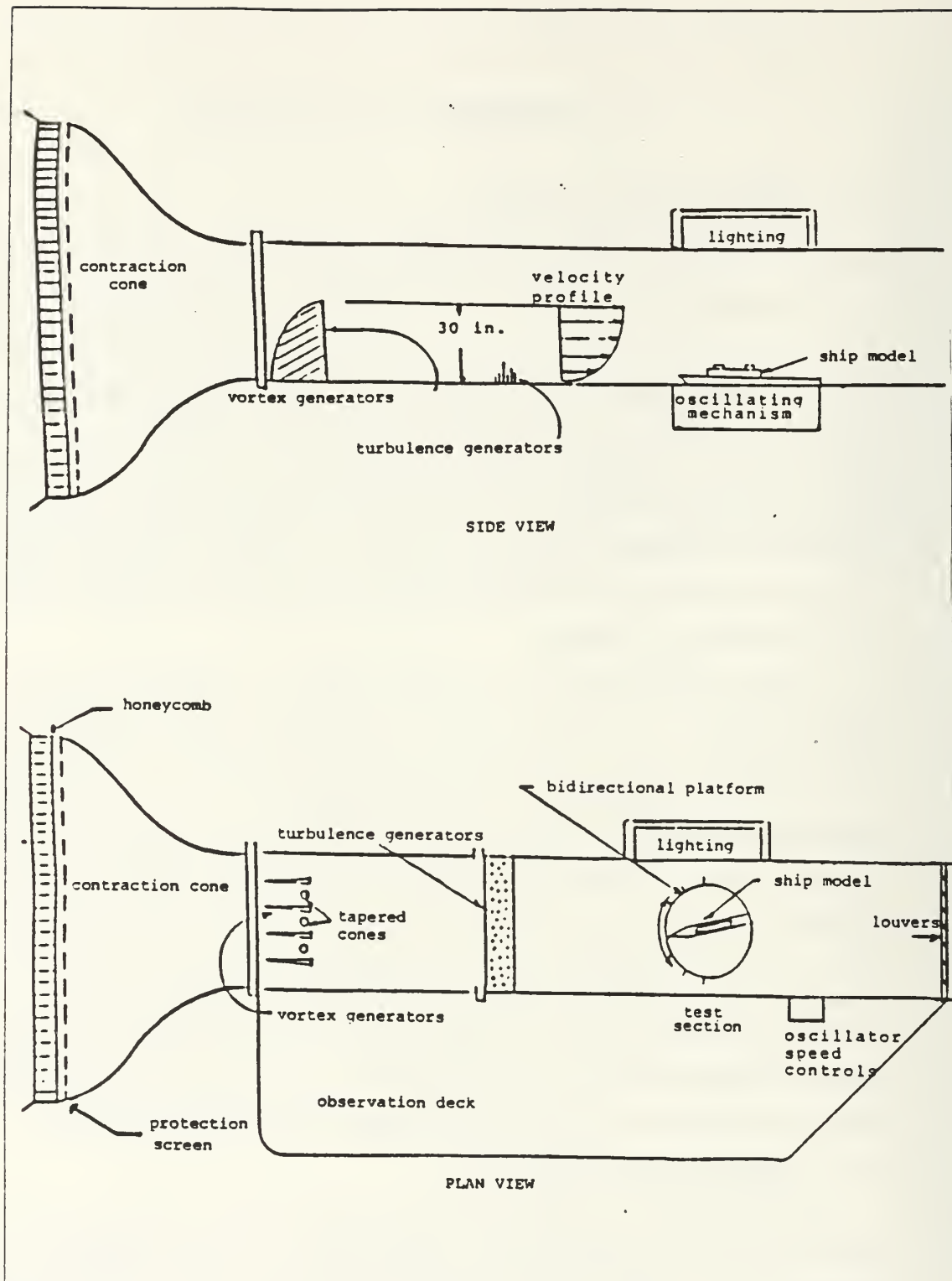
19

Figure 4.1 NPS Flow Visualization Tunnel.

20

probe. One hundred forty-four data positions were measured in the test section area, with sixteen horizontal and nine vertical coordinates. It is noted here that this thesis deals primarily with flow visualization techniques and its associated theory. A concurrent report written by LCDR Gary Selman deals with the data acquisition portion, thus any further details in this aspect may be obtained from that source. Tables 2 and 3 from Reference 9 are included here for continuity.

C.   OSCILLATING MECHANISM

It was decided to simulate only the highest-amplitude motions, as was discussed earlier, separately and then to investigate any non-linear coupling effects between modes. Thus the mechanism was designed to sustain heave, pitch, and roll or combinations of heave with roll and pitch with roll. The device incorporates two "Scotch Yoke" mechanisms connected by two joined shafts, and two motors (one for rolling motion, the second driving the yokes for pitch and or heave motions), which are mounted to a frame and centered just below the test section.

A five-amp, 1 2-Hp. Minarik motor controlled the vertical motion, using a belt to rotate two connected shafts, in turn driving the two yokes mounted to either end of the model. The Scotch yoke consists of a cylindrical flange with an eccentric pin, adjustable along the radius of the flange. The pin slides along the channel of the yoke, which is driven vertically by the pin as the flange is rotated (see Fig. 4.2). The yokes were maintained in the true vertical by Teflon guides. The two shafts connecting the yokes were connected at a coupling to facilitate transition from heave to the pitch modes. They were easily disconnected at the coupling and could be rotated through 90-degree phase increments, where in-phase represented pure heave and 180-degrees delineated the pure pitch. A pitch and heave combination mode was available at the 90- and 270-degree phase positions but was not analyzed for this experiment.

The roll mode was driven by a 1 8-horsepower, 1-amp Bodine motor, again using an eccentric cylindrical flange, but here it was connected directly to a control arm which fed into a pin through the center of the model. Both the flange and the arm length could be adjusted to provide desired roll angles, ranging from approximately 5- to 20- degrees. The roll arm connection to the model was by a simple pin, which was easily removed to shift to non-rolling modes.

As alluded to earlier, the model was to be analyzed in a flow with variety of yaw angles, ranging from zero degrees (head-on to the bow) to 35 degrees either side of the bow (a full range of motion through 360 degrees was available, but does not practically

TABLE 2
TEST SECTION VELOCITY DATA (FT/SEC)
(FROM REF. 9)

	Z- Height above floor (inches)								
X*	2.00	3.00	4.00	8.00	12.00	16.00	19.00	25.00	30.00
6.00	6.21	6.36	6.63	7.81	7.84	8.13	8.44	8.61	9.15
9.00	6.32	6.35	6.84	7.89	7.78	8.00	8.40	8.60	9.23
12.00	6.24	6.40	6.88	7.83	7.80	8.09	8.37	8.65	9.16
15.00	6.29	6.39	6.78	7.65	7.88	8.25	8.40	8.65	9.21
18.00	6.23	6.41	6.58	7.53	7.90	8.17	8.41	8.43	9.07
21.00	6.34	6.43	6.70	7.80	8.05	8.16	8.53	8.59	9.27
24.00	6.30	6.13	6.74	7.79	8.01	8.09	8.49	8.51	9.24
27.00	6.28	6.26	6.85	7.77	7.96	8.05	8.41	8.60	9.01
30.00	6.24	6.22	6.77	7.85	7.89	8.01	8.28	8.58	9.21
33.00	6.22	6.30	6.65	7.79	7.84	7.98	8.38	8.56	8.96
36.00	6.31	6.10	6.71	7.56	7.78	8.06	8.43	8.64	8.91
39.00	6.29	6.17	6.74	7.66	7.80	8.09	8.44	8.59	9.21
42.00	6.26	6.20	6.72	7.76	7.82	8.07	8.34	8.57	8.98
45.00	6.33	6.37	6.83	7.76	7.85	8.06	8.34	8.63	9.03
48.00	6.25	6.34	6.73	7.84	7.95	8.27	8.38	8.64	8.83
51.00	6.25	6.27	6.79	7.77	8.01	8.24	8.44	8.77	9.08
AVE.	6.27	6.29	6.75	7.75	7.89	8.11	8.41	8.60	9.10
V/Vo	0.68	0.69	0.74	0.85	0.87	0.89	0.92	0.95	1.00
SIGMA	0.04	0.09	0.08	0.09	0.08	0.08	0.06	0.07	0.13

Vo at 30 inches = 9.1 ft/sec
* transverse position from far wall in inches

22

TABLE 3
TEST SECTION % TURBULENCE INTENSITY DATA
(FROM REF. 9)

X*	Z- Height above floor (inches)								
	2.00	3.00	4.00	8.00	12.00	16.00	19.00	25.00	30.00
6.00	11.57	12.22	13.73	3.80	3.90	3.80	3.00	3.10	1.90
9.00	11.34	11.21	11.80	3.81	3.80	3.40	2.80	2.90	1.20
12.00	12.39	13.70	11.67	3.73	3.60	3.70	3.20	2.90	1.60
15.00	12.83	12.79	10.05	4.09	3.70	3.60	3.10	3.30	1.80
18.00	12.25	13.41	11.34	4.06	4.20	4.20	3.30	4.10	3.00
21.00	11.00	13.83	8.90	5.20	3.80	3.80	3.60	2.90	2.11
24.00	11.27	12.70	12.78	6.07	4.00	3.80	3.50	3.70	1.80
27.00	11.21	10.84	10.16	5.59	3.80	3.60	3.50	3.10	2.40
30.00	11.68	12.72	11.71	4.53	3.77	3.40	2.90	2.80	1.90
33.00	11.77	11.03	11.07	5.05	3.90	3.60	2.70	2.80	2.50
36.00	11.41	11.58	9.38	6.21	4.30	3.60	3.20	3.30	2.70
39.00	12.26	11.33	9.58	5.55	4.50	3.90	3.40	3.60	2.30
42.00	12.74	12.09	12.75	4.70	3.80	3.67	3.30	3.40	2.80
45.00	12.09	12.11	10.96	4.80	3.90	3.50	3.60	3.20	2.50
48.00	12.47	12.76	12.48	4.70	3.80	3.60	2.90	2.70	2.40
53.00	11.26	12.67	12.98	4.80	4.00	3.50	3.90	3.10	2.20
AVE.	11.85	12.32	11.33	4.79	3.92	3.66	3.24	3.18	2.19
SIGMA	0.56	0.90	1.37	0.76	0.22	0.19	0.33	0.37	0.47

Vo at 30 inches = 9.1 ft/sec

* transverse position from far wall in inches

simulate typical at-sea operations). It was desired that the entire oscillating mechanism could be rotated, and so it was mounted on a column attached to the center of the frame, with a locking handle to prevent any undesired rotation during the experimental runs.

D.   THE SHIP MODEL

In this preliminary phase of analysis, it was decided to use a generic destroyer model with relatively simple geometric shapes to simulate the deck levels and the superstructure, vice a more specific model type such as those listed in the introduction. In this way it was hoped to gain some foresight in coupled-mode effects and general characteristics of trailing vortex generation, particularly directly above the after-end area where most helicopter platforms are installed.

The following desireable characteristics were considered in determining the model composition:

(1)   ease of construction (since it was originally envisioned to use numerous generic models, examining affects of subtle changes of geometry)

(2)   durability (to withstand a variety of oscillation frequencies up to three Hertz)

(3)   lightweight (for minimal strain on the mechanism's motors and to reduce effects of dynamic loading)

(4)   low cost (always a driving factor)

Also, it was desired to yield easily to modifications, such as the addition of vent holes for smoke aerosol injection. Of the materials considered, polyurethane foam of medium density (8 lbs cubic ft) met all the characteristics listed. Surfaces sanded relatively well with a sealant applied, and a flat black lacquer could then be directly sprayed to the exterior. This low-reflective coating was desired for optimum contrast during photography, and was therefore also used inside the entire test section area of the wind tunnel.

The platform consisted simply of a 5-foot diameter plywood disk cut out of the tunnel floor at the center of the test section. The model shape was then cut into the disk with approximately a half inch gap for model clearance in the rolling mode. A minor obstacle in implementing this system occurred when attempting to prevent ambient air from entering the test section through the gap between the model and the cutout in the disk. Commercial types of bristle and closed-cell polyurethane weatherstripping proved inefficient due to lack of compressibility. The commercial foam with a self-adhesive strip also tended to peel off the cutout edges during extended
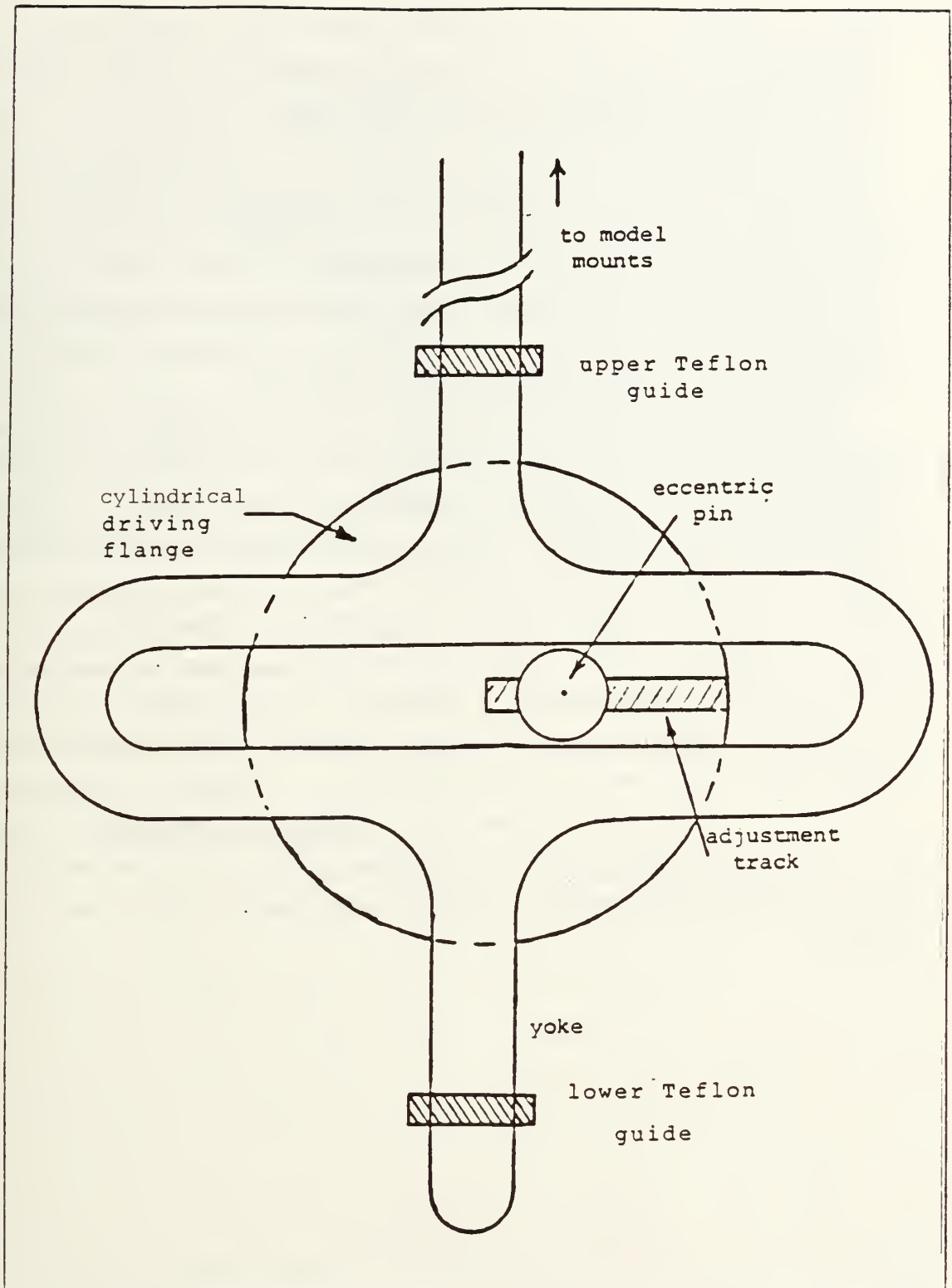
Figure 4.2 Scotch Yoke Mechanism.

periods of oscillation. The best results were obtained with a lower density (open-cell) polyurethane (the type found in seat cushions) attached to 1-1 4-inch wide batting strips along the cutout edge. A good contact cement was used, and the batting provided a larger surface area for bonding than did the 3 4-inch unmodified disk. This provided a sufficient barrier to unwanted flow caused by the pressure differential during the wind tunnel operations. Finally, the disk was reinstalled and supported by circular sections of steel plate mounted to the underside of the tunnel floor, making it easy to rotate the model disk oscillating mechanism system through any desired yaw angles. The disk was also clamped at three positions from underneath to ensure it was maintained level with the remainder of the test section floor.

Both the motors were controlled by variable-speed Minarik voltage control boxes, which were mounted on the outside of the tunnel wall but inside the observation deck (see Fig. 4.1). The desired rotational speeds were verified by a Monarch Instruments TACH IV electronic tachometer, which operates be directing a collimated light beam onto a reflective marker attached to either the yoke (for measuring the pitch mode) or the outside of the cylindrical flange (for roll). The reflected pulses are compared against a 6-MHz. internal crystal timebase, and the resultant speed measurement is displayed directly in RPM on an LED readout. The instrument incorporates a microprocessor to compute the time interval between successive reflected pulses, which were received be either directly pointing the instrument at the reflective markers or by using a remote sensor. The last option was the most preferred since it was not required to leave the observation room to take the measurements under the wind tunnel, and the controllers could then be adjusted with real-time feedback.

V. EXPERIMENTAL METHODS

A. FLOW VISUALIZATION TECHNIQUES

Numerous techniques are available to the aerodynamicist for the enhancement of qualitative flow study. As with all engineering situations, each has its own benefits and drawbacks depending on the requirements of the problem. Flow visualization may be approached from two major areas, that of on-body analysis and that of off-body, or the area surrounding the body in study. A common dilemma to both areas of on-body and off-body analysis is that it is imperative that a negligible disturbance to the flowfield be introduced to ensure accurate results are obtained. As an example, compare the flow visualization aspect to the data acquisition portion of the project. A pitot-static probe may be used nearly anywhere in the test section (except very close to the model and tunnel walls due to mutual interference) to determine the freestream velocity, but any area downstream of the probe cannot be evaluated concurrently unless the exact disturbance effects from the probe are known and can be corrected for in the data reduction. Likewise, any flow visualization techniques introduced to the flow, whether on-body or off-body, must not alter that which it is attempting to analyze.

1. On-body Flow Techniques

This is the area immediately surrounding the model, and all current techniques utilize some sort of application. Techniques considered here included oil and clay smears and tufting. The smears would provide a long term record of the local streamlines, photography would be less critical and the flow around the entire model could be analyzed in detail, but at the low speeds used in this study the required streaking would probably not occur. Previous work by LCDR Bolinger for the static model entailed the utilization of very thin fluorescent nylon filaments (0.7-thousanths of an inch in diameter). These tufts were attached in an evenly spaced in a grid along the model, with application procedures detailed in [Ref. 9: pp. 32-33]. Due to their small size and flexibility they had virtually no influence on the flowfield, and the dynamics of the local streamlines were easily traced, as seen in Fig. 5.1. Due to delays in model construction and implementation, this technique was unable to be used with the oscillating model.
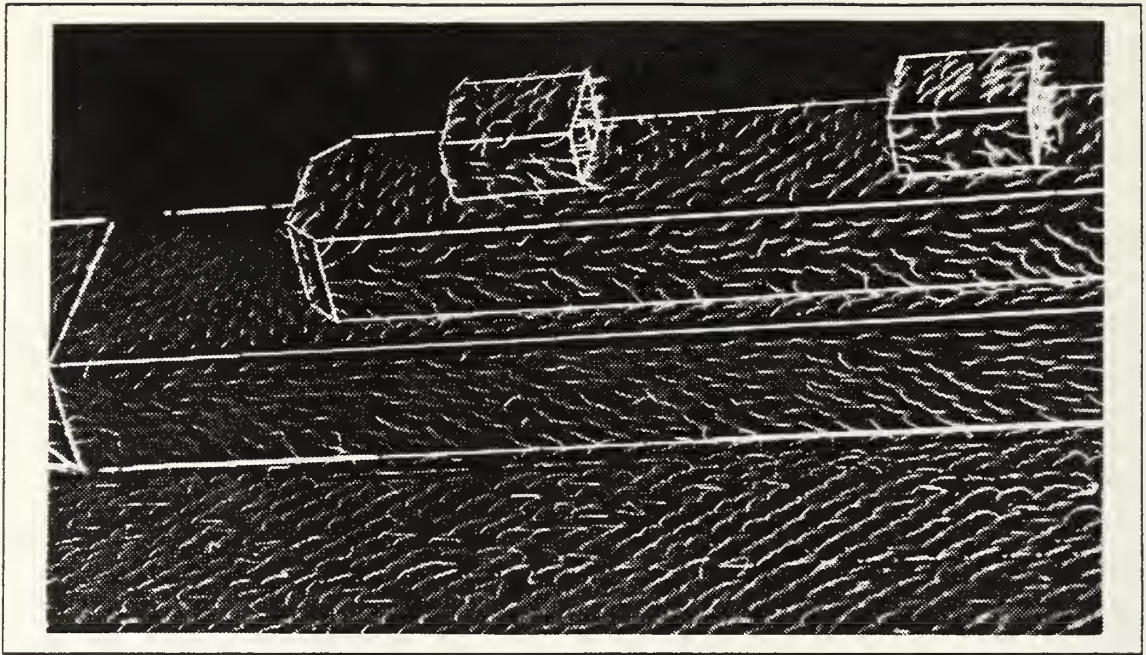
Figure 5.1   Example of Fluorescent Minitufts, Static Model.

2. **Off-body Flow Techniques**

These methods typically employ the injection of light-scattering particles into the flow, acting as tracers to the flow streamlines. The particles should be of a sufficiently small size, at most around a hundred microns, so as to introduce no disturbances to the flow but must still be able to disperse the light for visualization purposes. Two methods were used.

An exception to the particle size was employed, consisting of neutrally-bouyant helium bubbles ranging in sizes of one to three millimeters in diameter. Mueller [Ref. 11] provides a detailed description of a similar bubble generating system and lists several applications he encountered during his research in flow visualization methods. This technique was attractive because bubbles could trace individual streamlines of the flow, and also because the quick dispersion of the substance in moderate turbulence was not experienced as it is in smoke techniques. Helium bubbles were created using a Sage Action, Inc. (SAI) system, which consisted of a bubble generator console, an ejector head, and a vortex generating chamber (see Fig. 5.2). The console controlled the bubbles size, density and generation rate by a mixture of soap-film solution and helium, with 50-psi air used to drive the bubbles through the

28
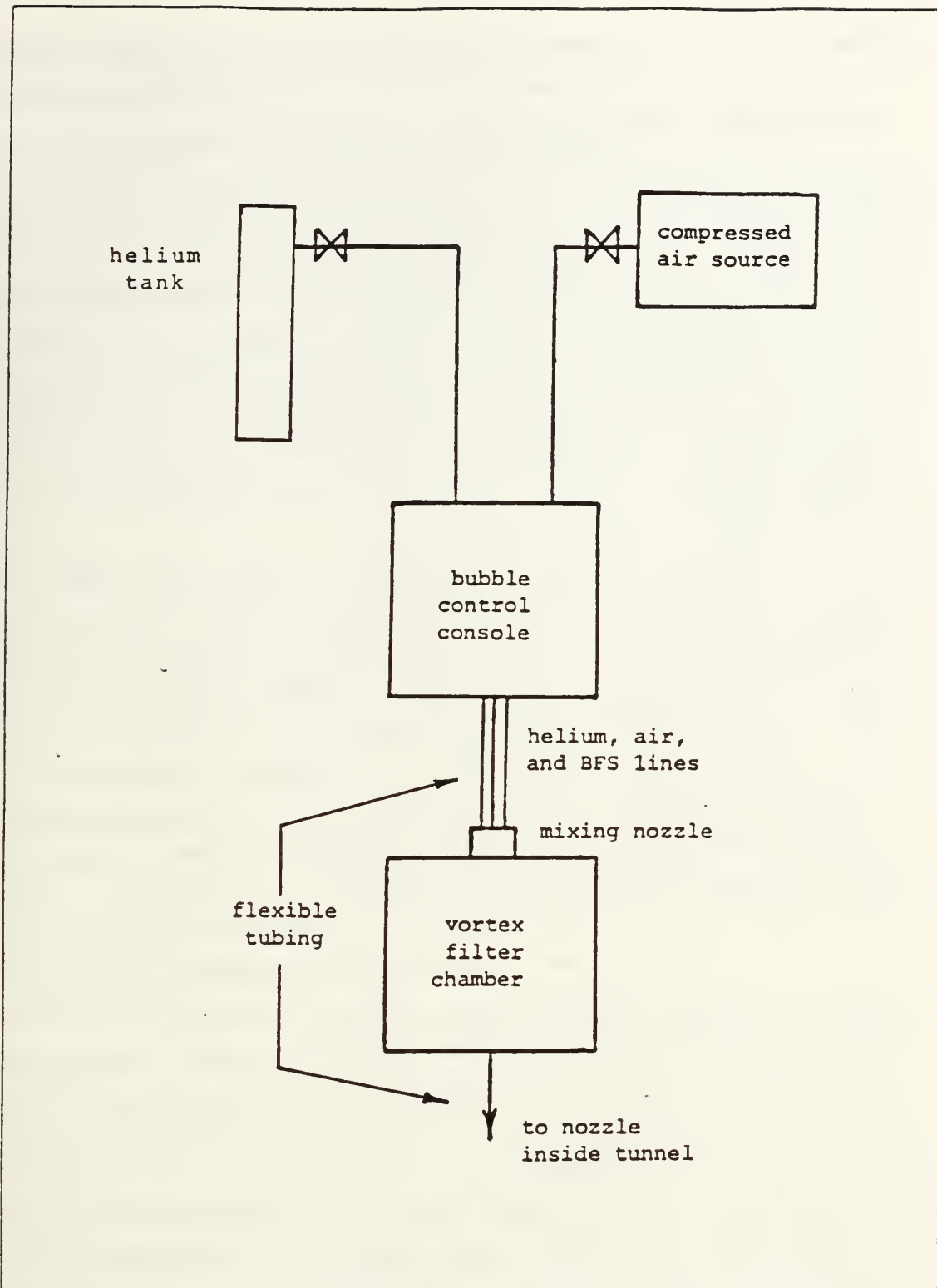
Figure 5.2   Schematic of Bubble Generating System.

29

helium, with 50-psi air used to drive the bubbles through the chamber. The bubbles were created at the ejector nozzle and fed directly into the vortex generating chamber, where the lighter bubbles impacted the outlet tube in the center of the chamber and the heavier bubbles impacted along the walls of the chamber. This allowed the truly neutrally-bouyant bubbles to pass through the vortex generator and be directed through flexible tubing into the tunnel's test section approximately 18 inches upstream of the model. A nozzle was used to direct bubble flow downstream, and since the pipe supplying the nozzle replaced existing dowels in the tunnel it had no effect on the turbulence intensity already calculated. The nozzle was supplied from the underside of the tunnel, and could be placed at a variety of spanwise locations depending on the model yaw angle and the desired area of flow analysis on the model. This system produced excellent results for the static model analysis and good results for the oscillating model.

Due to the relatively high Reynold's Number (about 50,000), another technique was attempted in order to obtain more detailed analysis closer to the model, particularly the superstructure areas. A small particulate substance was desired for the finer detail, with the realization that this type of material would be quickly dispersed. Smoke was to be avoided due to safety constraints and it was simply messy to work with. A liquid aerosol system described by Griffin and Ramberg [Ref. 12] was investigated and found to be quite appropriate for the purpose of this project. This system produced a fine mist which was discharged from strategic areas of the model, especially the areas of shed vortices determined from the static analysis. The system described by Griffin was easily modified to existing units of the helium bubble generator system from SAI, thereby making it easy to implement. The compressed air tube was disconnected from the generator console and routed to the inlet of the liquid DOP {di(2-ethylhexyl)-phthalate} agitation chamber; the output was then connected, again by flexible tubing, to a jet impactor nozzle inside the drum used as the vortex generator for the bubble system. The jet impactor was used to reduce the particle size and enable the smaller particles to follow the unaffected flow. The output of the chamber then went to a brass manifold with six outlets, from which tubing was run to the various areas of the model described earlier. All connections between major components of both systems were with flexible tubing except for the aerosol exhaust ports which consisted of brass piping through the model and connected to tubing on the model's underside. The DOP was an ideal substance, since it is chemically inert,

non-toxic, non-corrosive, the system requires no chemical reaction or combustion, and it contains no moving components for very little maintainance.

B.   PHOTOGRAPHIC TECHNIQUES AND LIGHTING

Each flow visualization technique required somewhat different photographic methods and therefore different lighting schemes were necessary for optimum results. With only a few exceptions, the photographic equipment used was a single-lens reflex Hasselblad 2000-FCW camera with one of two Hasselblad lenses: either a 110-mm. or a 150-mm. The Hasselblad is a professional-format camera, which was desired for better resolution on enlargement printing. It became normal procedure to shoot with 3000-speed, type-107 black and white Polaroid film initially to ensure proper exposure, then the final photography was done using Kodak TMAX 400 professional film. To account for the difference in film speeds, the TMAX was exposed by opening the aperture one "f-stop" and overdeveloping ("pushing") the film two stops. Other types and speeds of both color and black-and-white films were evaluated, but the best contrast was most consistently obtained with the Kodak TMAX. In all cases, proper lighting was the primary obstacle, due in large part to the restrictive confines of the observation photographic deck and the limited size of the plexiglass viewing ports in the walls and ceiling. Also, any wind tunnel is faced with the problems of blockage and interference, so discretion had to be maintained in the placement of any illuminating devices inside the tunnel itself, particularly upstream of the test section. The reference used for all photographic techniques and procedures was *Handbook for Scientific Photography*, by Alfred Blaker [Ref. 13]. The specific techniques employed are now discussed in the following text.

1. Oscillating Model with Aerosol

It was much more difficult to obtain usable photographs when the aerosol flow visualization technique was utilized. The lighting procedures first attempted are similar to those discussed by Griffin [Ref. 12: p. 68], in which the camera shutter was held open in a blacked-out room and the exposure was determined by the back flash set on the opposite side of the tunnel. The flash unit used was a Norman 2000, capable of various power levels from 400 to 2000 W-secs., and the head was flashed through a honeycomb screen for directionality. The full range of flash power settings were also explored. In an attempt to bring out more contrast in the photographs, K-2 (yellow) and A (red) filters were used for many of the shots, in accordance with Blaker [Ref. 13: pp.69-79]. Another effort entailed using Kodak Ectachrome color slide film

flash techniques combined with fast shutter speeds were initially desired to "freeze" the motion of the ship during oscillation, with a wide range of aperture settings and shutter speeds examined.

2. Static/Oscillating Model with Helium Bubbles

This method produced the best photographic results of the three flow visualization techniques used. Since the desired end result was to obtain bubble streaks which followed the flow, extended shutter speeds were required. The lower end of the scale (fastest shutter speed) was at 1/4-seconds, with any faster speeds than that giving short traces and little practicality of analysis. The upper end was at 2-seconds, since slower speeds produced so many traces that the overlap was too great to be able to follow any one particle. The best results were obtained with a shutter speed of 1-second for the static case and 1/2-second for the oscillating runs, with aperture settings between F-4 and F-8/11 (depending on the lighting scheme).

The bubbles showed up best when being illuminated against a totally dark background, so the lighting was set up to cast as little light as possible onto the model. This became quite challenging at times in view of the fact that the model was three dimensional and of irregular shape. The source of lighting which produced the highest trace intensities was an EIMAC model R-150-5 high-voltage arc lamp placed inside the tunnel and well downstream of the model. This was used to either direct a circular beam along the port (left) side of the ship, which in all cases was the viewing photographic side, or around the entire model. The latter case worked better for the static nose-down runs and some of the oscillation shots. Due to limitations with lateral working space inside the tunnel, combined with the arc lamp being housed in a three-foot long shroud, the runs at a 35-degree yaw angle required the beam to be bounced off of a mirror attached to the tunnel wall. Adjustment was time consuming, but once in place the effect was substantially improved with the arc lamp.

The arc lamp, however, provided illumination in limited areas, and interesting sections of the flow, such as between the stacks or behind the superstructure, required alternate lighting with good directional versatility. It was found that slide projectors served this purpose quite well. Two types were used, a Kodal Ectagraphic Model AF-2 and a 500-W Sawyers "Rotodisc" projector, with three to six being used at any one time depending on the areas of interest surrounding the model. Normally, two or three were used on the opposite side of the tunnel to illuminate the areas of the bow and stacks, with the remainder positioned at various angles inside the tunnel aft of the test

section. An 800-Watt professional theatre lamp was occasionally used, but was bulky and was difficult to accurately direct around the model inside the confines of the wind tunnel. The projectors could provide a large area of lighting, say over the top of the model or along the starboard side, otherwise they were used with slides to create highly detailed beams to completely silhouette the ship. These slides were manufactured from strips of aluminum tape with the shape of the lighted area being cut out, and since construction was relatively easy numerous were made and could be changed at convenience (for example, after a change of yaw angle). This method provided excellent results for the static cases, but the set-up time was normally quite long and laborious.

The oscillating runs presented more of a dilemma: the lighting could be optimized for only one position, but the model motion caused some areas to be unlit at one part of the cycle and producing excessive model glare at other parts. A compromise was made to reduce some of the illumination areas very close to the model and accept some occurrences of glare. It is noted here that substantial blur due to the ship movement was anticipated but would be accepted since the actual subject matter was the bubble traces themselves. Moreover, it was hoped to determine the ship position from the blur through various stages of its cycle.

VI. RESULTS

The flow visualization methods which were utilized in this study have been described in detail, along with their associated photographic and lighting techniques. The following results are first discussed according to the flow visualization method (as in Chapter V), with the helium bubble section subdivided by yaw angles. It is noted, and will become obvious as the figures are scanned, that it was the bubble technique from which the conclusions were derived.

The tunnel freestream velocity was held constant at 9.1 feet per second for all of the test runs. From the data of Table 2, the freestream velocity can be computed for various heights of interest. For example, the velocity over the bow (at $z = 2$ inches) was approximately 6.25 ft/sec., or at the top of the stacks (at $z = 4.5$ inches) it was approximately 6.9 ft. sec.

The pictures presented here are representative of a much larger grouping from which the observations and conclusions were made. These are published solely as an example of the results obtained and to help illustrate the validity of the conclusions being drawn. It is also noted that much of the resolution from the original photographs was lost during the printing process.

A. AEROSOL INJECTION

The results for this technique can only be described as disappointing. In attempting to use a high-powered flash from across the tunnel, the results were inconsistent and were very sensitive to the angle of the flash head with the honeycomb attachment. Without the use of the honeycomb the pictures were extremely overexposed, even at the lowest power settings for the flash and the highest aperture settings on the camera. It is suspected that the flash head was quite prone to the vibration of the tunnel, causing it to become quickly misaligned.

The system plumbing is also suspected to be a contributor to the frustration caused be this method! Eighth-inch tubing was used to transport the aerosol through the ports, this may have been too restrictive to obtain a high-density flow. Thicker aerosol clouds were easily obtained by increasing the air pressure into the DOP agitation chamber, but this action produced relatively high velocity aerosol jets from the exit ports and thus made this trick invalid. Also, the regulator valve for the

34

compressed air inlet was very sensitive to adjustment and a consistent but yet realistic aerosol flow was difficult to obtain.
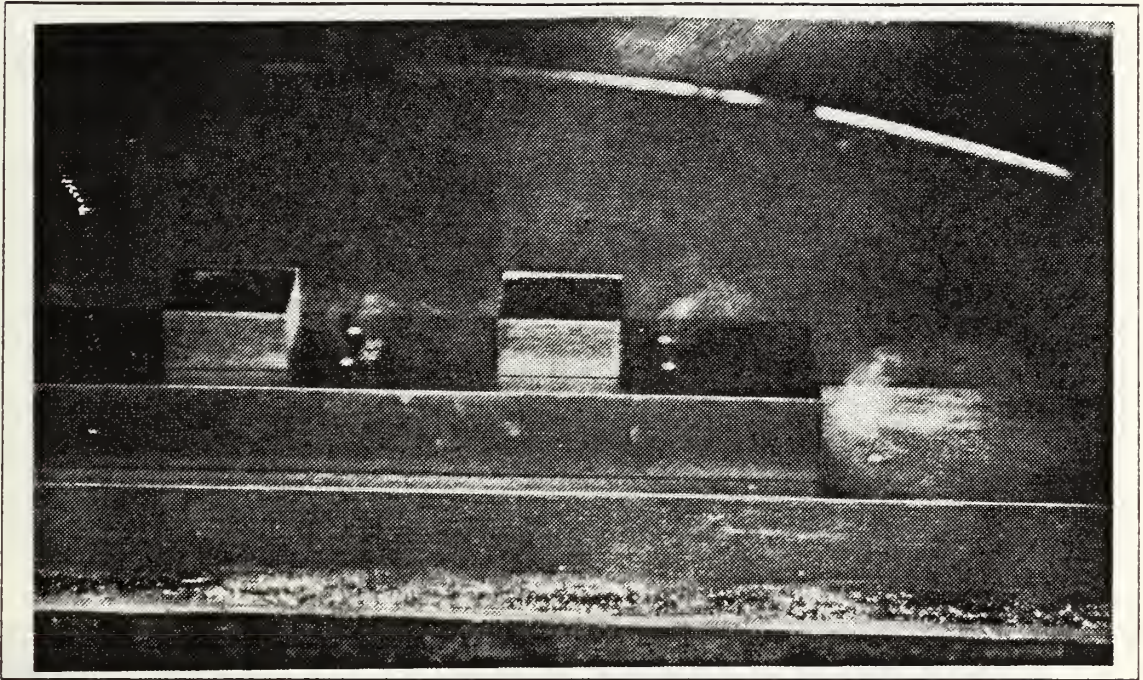
Figure 6.1   Sample Results with Aerosol.

The photo included here (Figure 6.1) was taken by the third technique described in the photographic procedures section, using Ektachrome color film for higher contrast. The difficulty generated from this technique may have been primarily from the glare received from the flash bouncing off of the plexiglass viewing port.

The aerosol injection technique continues to be modified as of the writing of this report, including possibilities of installation of larger diameter tubing and shooting the photographs from inside the tunnel to avoid any glare problems.

B.   HELIUM BUBBLE STREAKS

This method of flow visualization became the preferred analysis technique, since once the lighting problems discussed in Chapter V were overcome the procedure was straightforward and the results were consistent. At each yaw angle the model was photographed at the following positions:

(1)   Zero degrees for roll and pitch (true static condition)

(2)   Full left roll, zero pitch.

(3)   Full right roll, zero pitch.

35

(3)   Full right roll, zero pitch.

(4)   Zero roll, full nose down pitch.

(5)   Zero roll, full nose up pitch.

(6)   Oscillating model in both roll and pitch.

The above positions are defined as follows: full roll (left or right) is approximately 8 degrees, and full nose (up or down) is approximately 4 degrees. All figure titles are in reference to the above, in that "nose up" is assumed full nose up at 4 degrees and "left roll" refers to full left roll at 8 degrees. The photos of the oscillating model show that the ship is blurred, but the helium bubble streaks were generally quite clear. Numerous photos show distinct shaded columns above the two stacks. These are from the projector lighting at the opposite side of the test section, and were highly pronounced only on days when smoke visualization techniques were being used concurrently in other nearby facilities. Lastly, little difference could be seen consistently enough in the two different roll positions to draw any definite conclusions, thus only one roll position for each series of yaw angles is included in the following results sections.
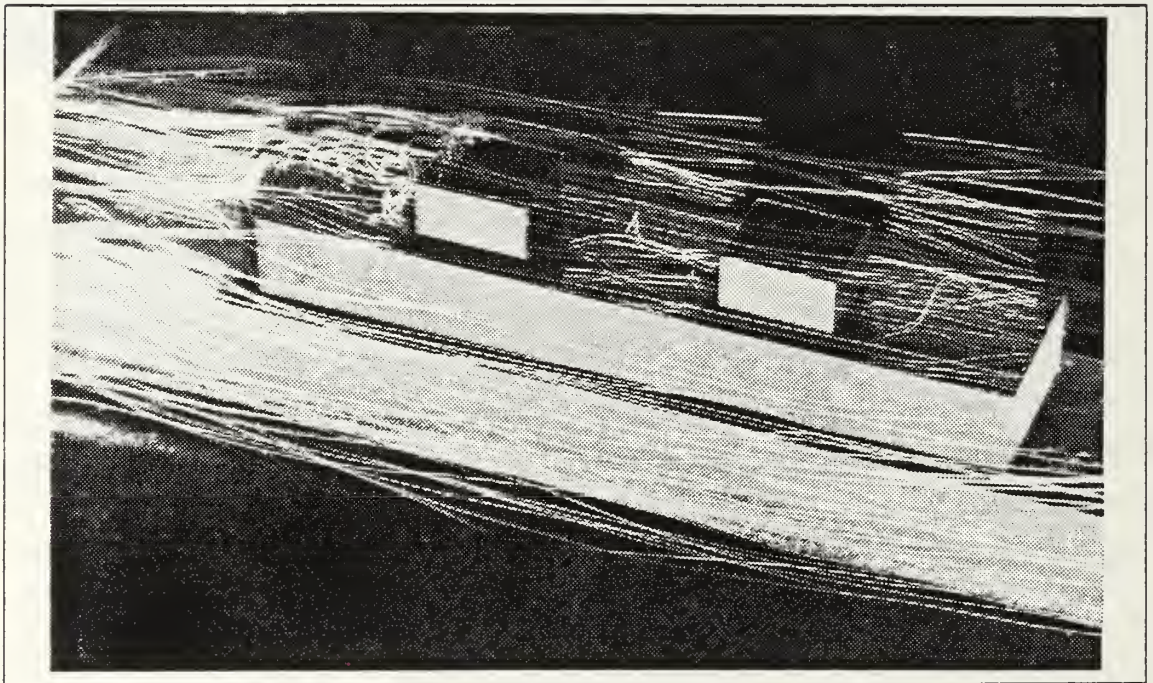
Figure 6.2   Zero Degrees for Roll and Pitch at Zero Degrees Yaw.

36

Figure 6.3   Left Roll at Zero Degrees Yaw.
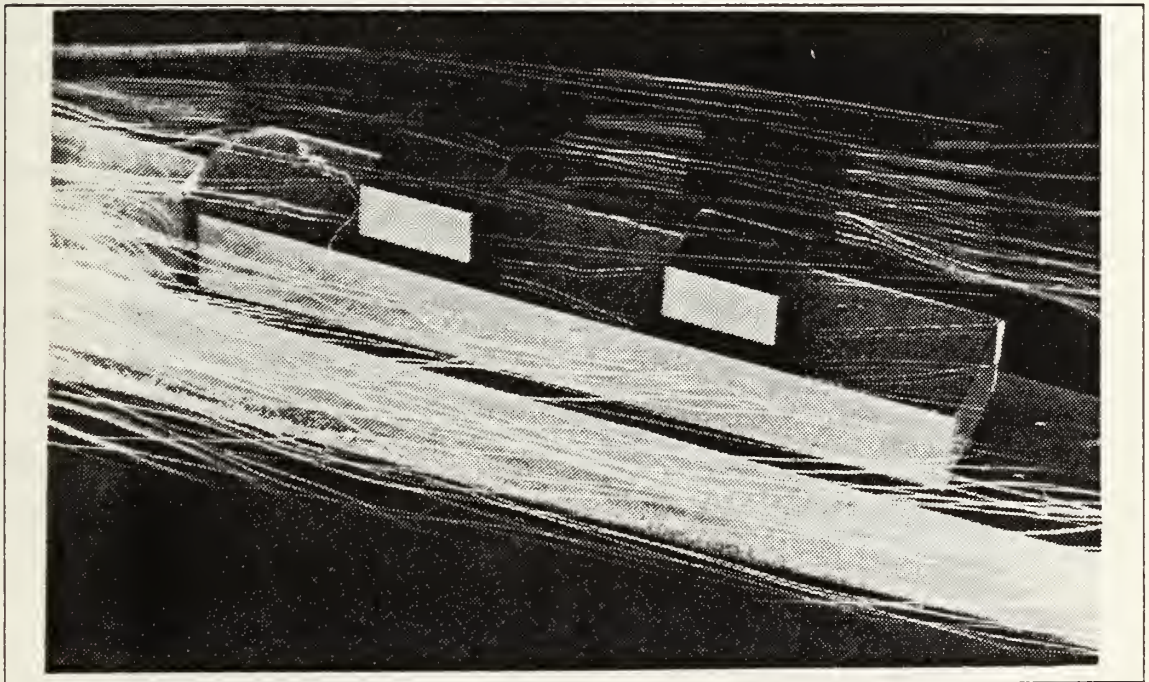
Figure 6.4   Nose Up Pitch at Zero Degrees Yaw.
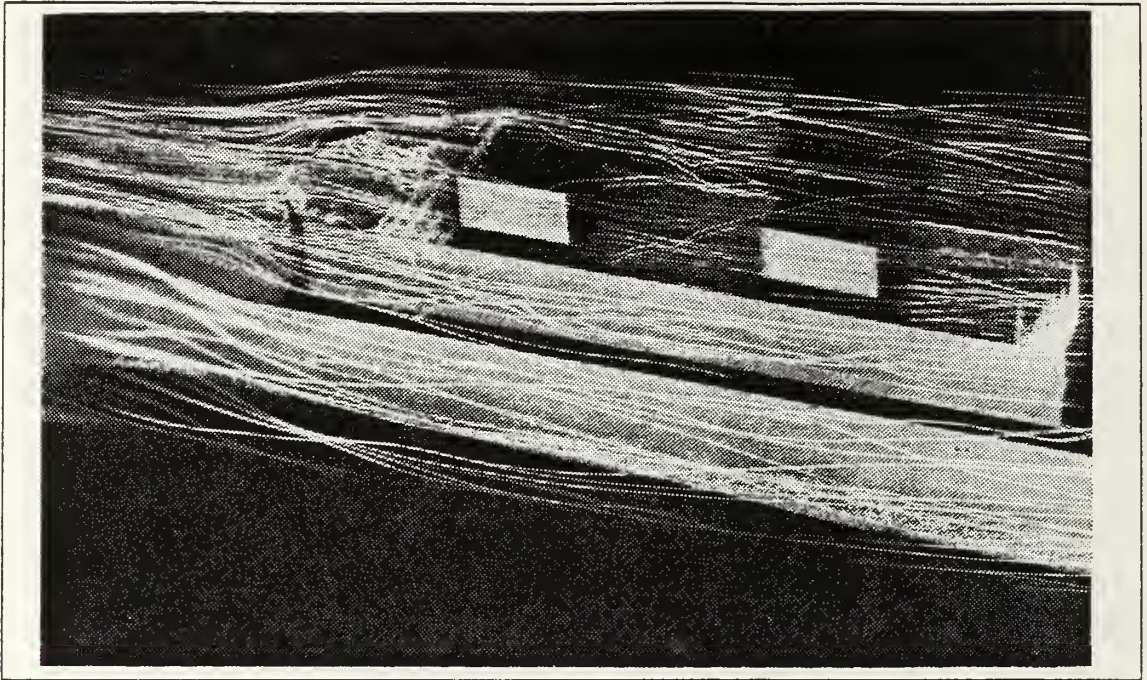
Figure 6.5   Nose Down Pitch at Zero Degrees Yaw.

1. Zero Degrees Yaw

The flow generally appears to be quite symmetrical along either side of the model, despite the existence of the turbulent boundary layer. Evidence of the recirculation zones, although negligible in Fig. 6.2, is seen behind the aft stack in Fig. 6.3. For the nose up case, not evident in Fig. 6.4, the flow has a very distinct detachment over the bow but quickly reattaches and has little affect on the superstructure and forward stack. As would be expected, the opposite is true for the nose down case (Fig. 6.5), with stronger trailing vortices being generated off the leading edge of the superstructure and forward stack. The oscillating shot (Fig. 6.6) has substantially fewer bubble traces due to the shorter exposure times, but displays some interesting features. A "wave affect" is seen on several traces along the port side, presumably due to the motion of the stacks, and the forward stack oscillation is shown by the series of inward and outward direction changes of several bubble traces.

38
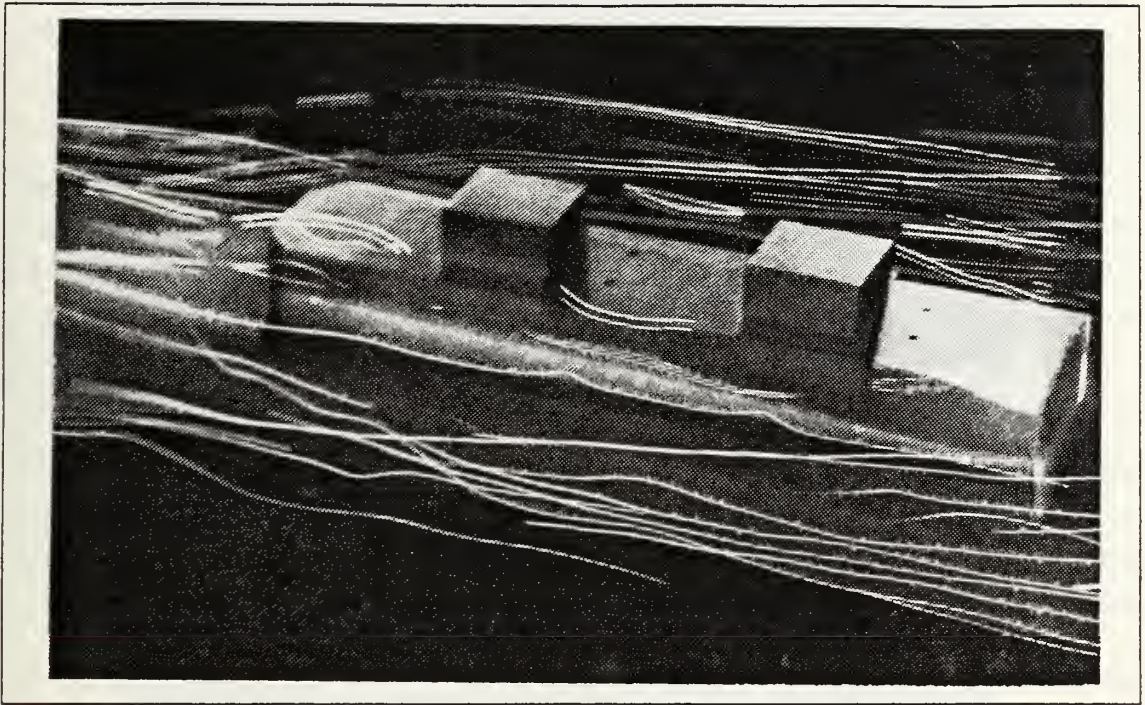
Figure 6.6   Oscillating Model at Zero Degrees Yaw.
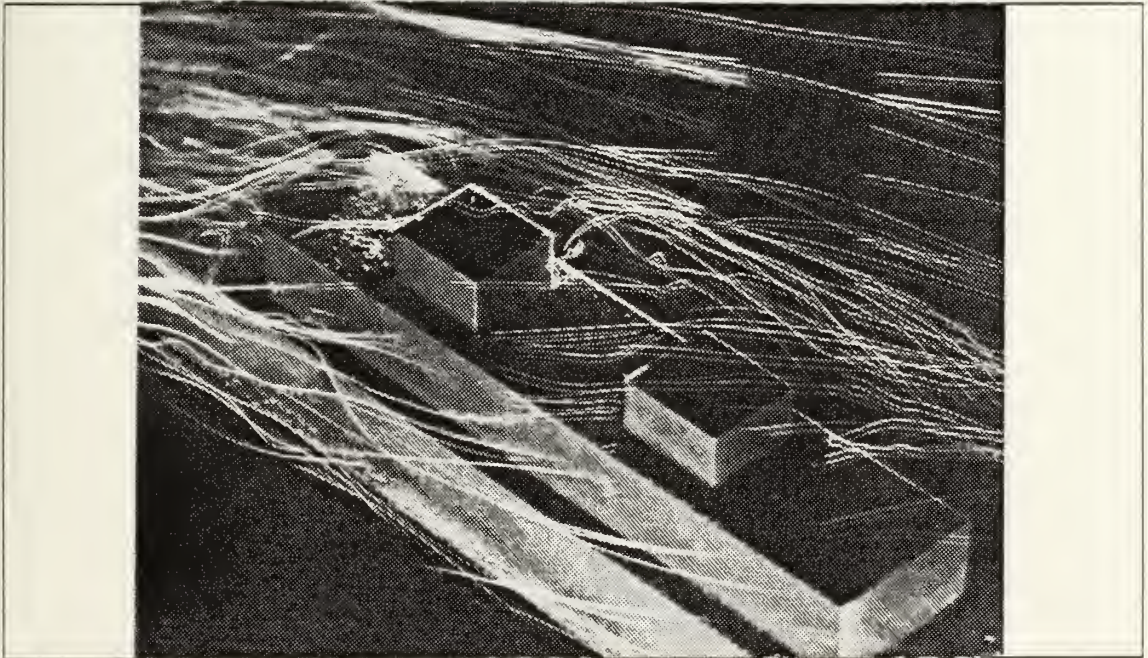
Figure 6.7   Zero Roll and Pitch at 20-Degrees Right Yaw.

2. Twenty Degrees Right Yaw

A foot vortex has generated just aft of the bow and travels along the lower port side leading-edge of the superstructure, with numerous weaker vortices trailing from various areas of the ship. The initial trailing vortex angles are the same as the model's yaw, but as they continue travelling downstream they realign themselves with the freestream and join together to form a single large vortex. Figure 6.7 shows the shift of the stagnant regions around the front stack. The left roll position (Figs. 6.8) shows a stronger trailing vortex at the aft end of the forward stack, again in comparison to the zero-degree yaw position, as well as the generation of a trailing vortex off of the edge of the superstructure. The pitch positions (Figs. 6.9 and 6.10, respectively) display effects similar to those seen at the zero-degree yaw position. The oscillating shot (Fig. 6.11) was chosen to show the effect on the recirculation zones: bubbles were still captured here and actually maintained oscillations with the model for a short time before escaping back to the freestream.
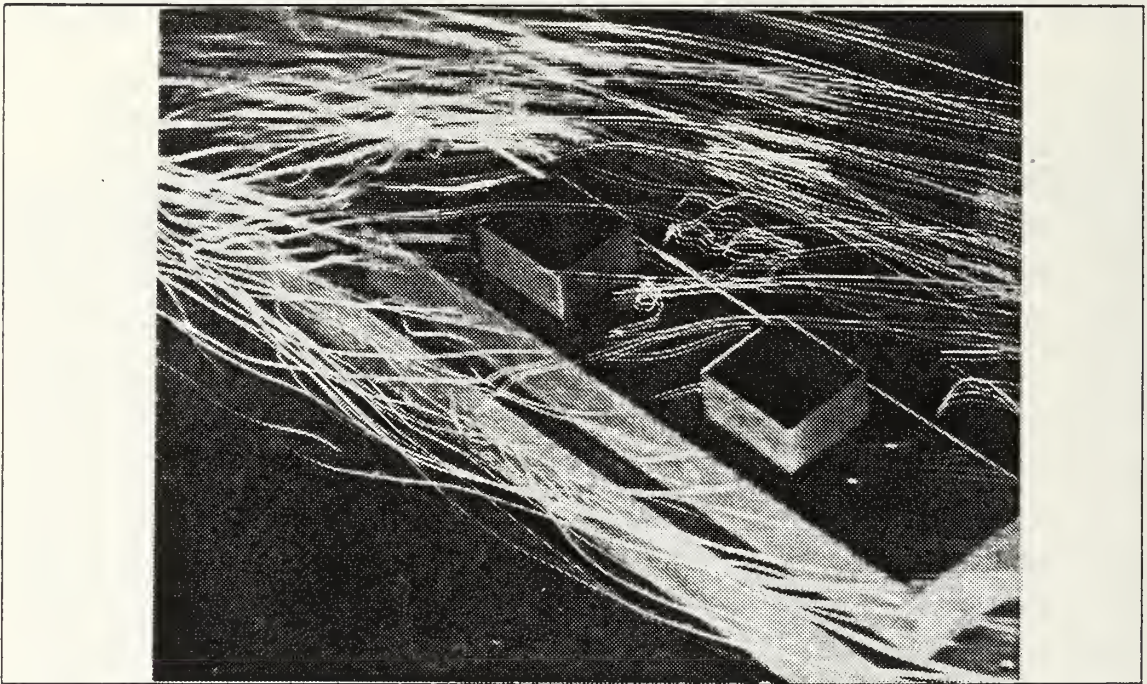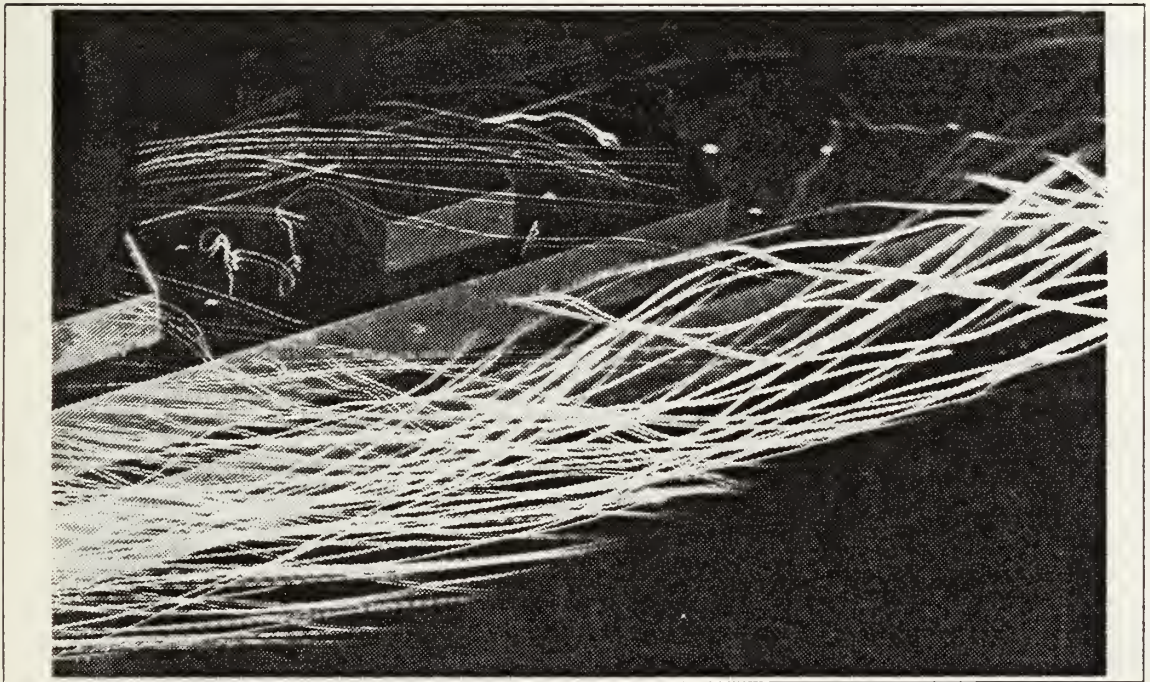

Figure 6.8   Left Roll at 20-Degrees Right Yaw.
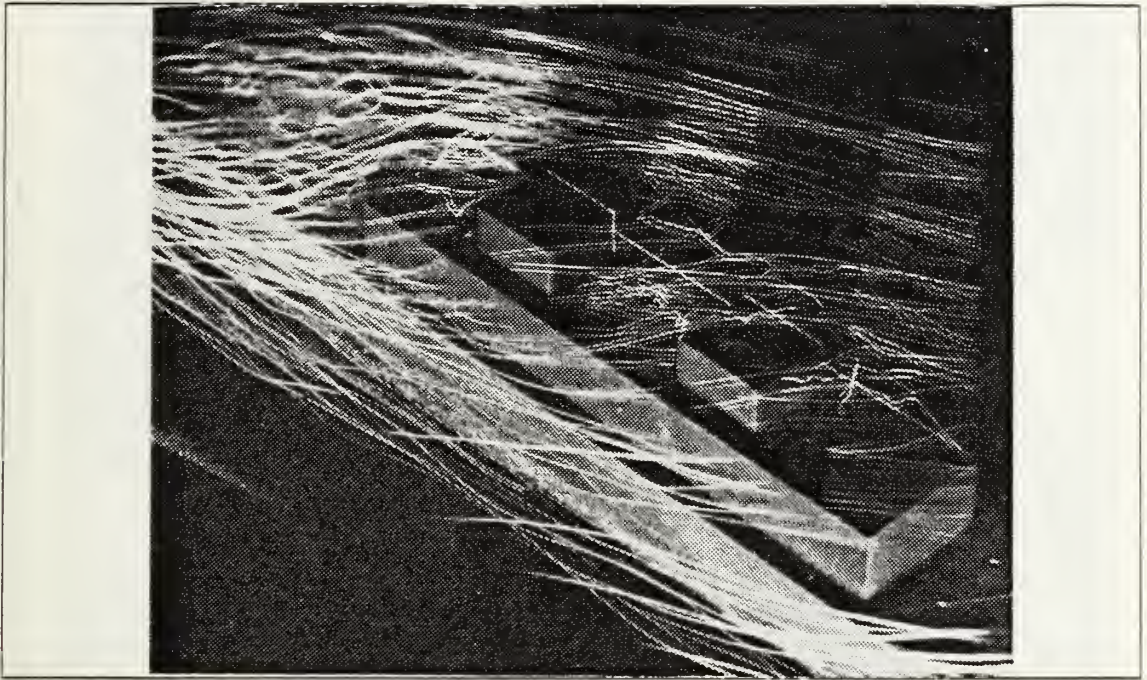
Figure 6.9   Nose Up Pitch at 20-Degrees Right Yaw.
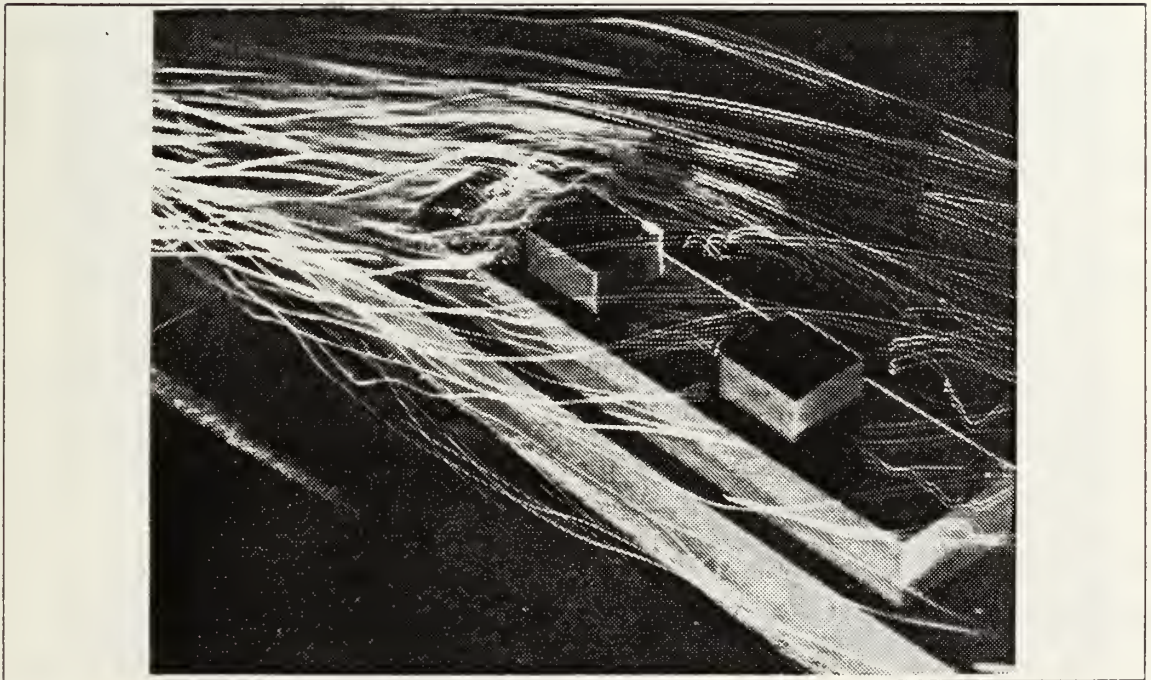
Figure 6.10   Nose Down Pitch at 20-Degrees Right Yaw.
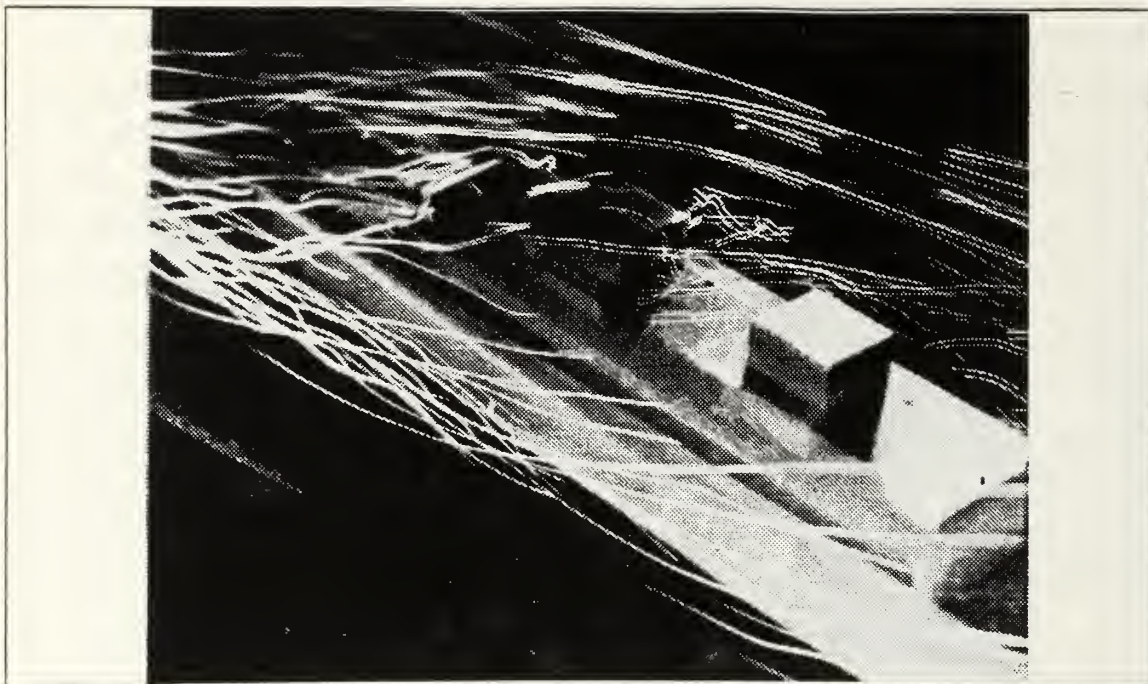
Figure 6.11   Roll and Pitch Oscillations at 20-Degrees Right Yaw.

3. Twenty Degrees Left Yaw

This position shows primarily a mirror image of the twenty-right yaw position (Figs. 6.12 to 6.16). More obvious from this aspect, however, is the development of the large corkscrew vortex on the leeward side. Of particular interest are the trapped bubbles in Fig. 6.12 directly behind the first stack, and the large area of detaching flow off the bow in Fig. 6.14. The bubble traces appear more irregular in Fig. 6.16, particularly along the port side, which may be attributable to the ship's oscillations.

4. Thirty-five Degrees Left Yaw

Trailing vortices are evident on most of the sharp edges of the model at this higher yaw angle (Figs. 6.17 to 6.21). The corkscrew vortex has grown even more in size, and the flow generally appears more turbulent throughout the entire flow field. The position at right roll (Fig. 6.18) shows the detaching of trailing vortices over the entire section before the superstructure. This effect is weakened in the nose down position, but much more prevalent with the bow up than has been seen at the previous yaw angles. The model in the oscillating mode (Fig. 6.21) displays more irregularities in the bubble traces than do the static modes, presumably due to the interaction with the ship's motion.
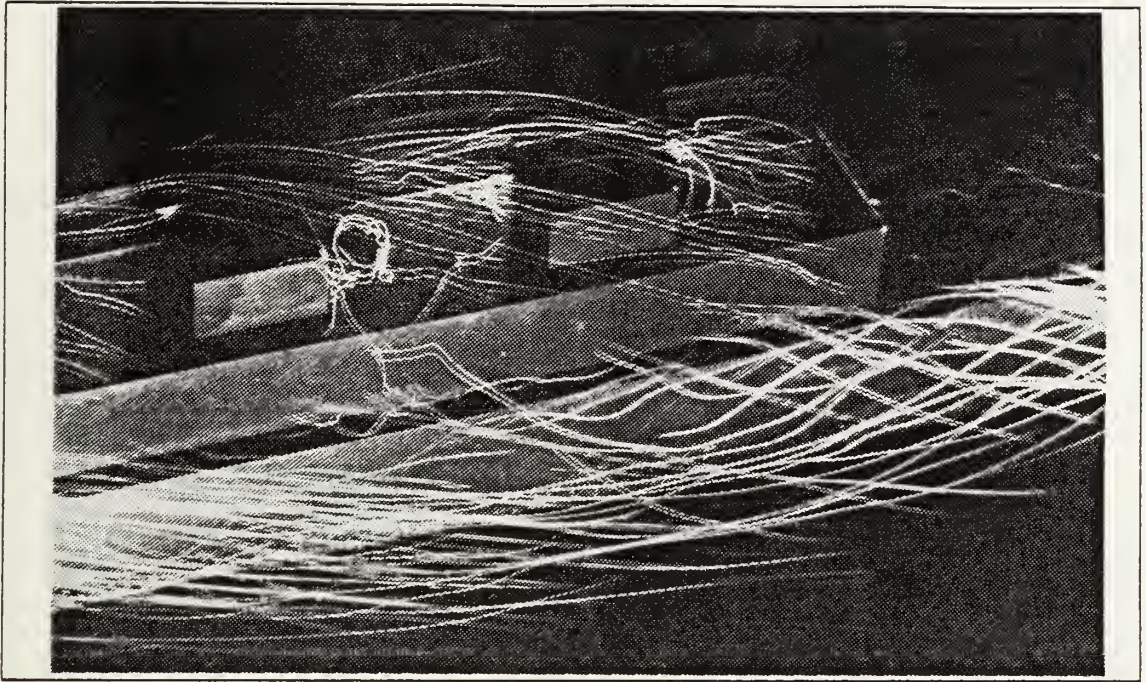
Figure 6.12   Zero Roll and Pitch at 20-Degrees Left Yaw.

Figure 6.13   Left Roll at 20-Degrees Left Yaw.
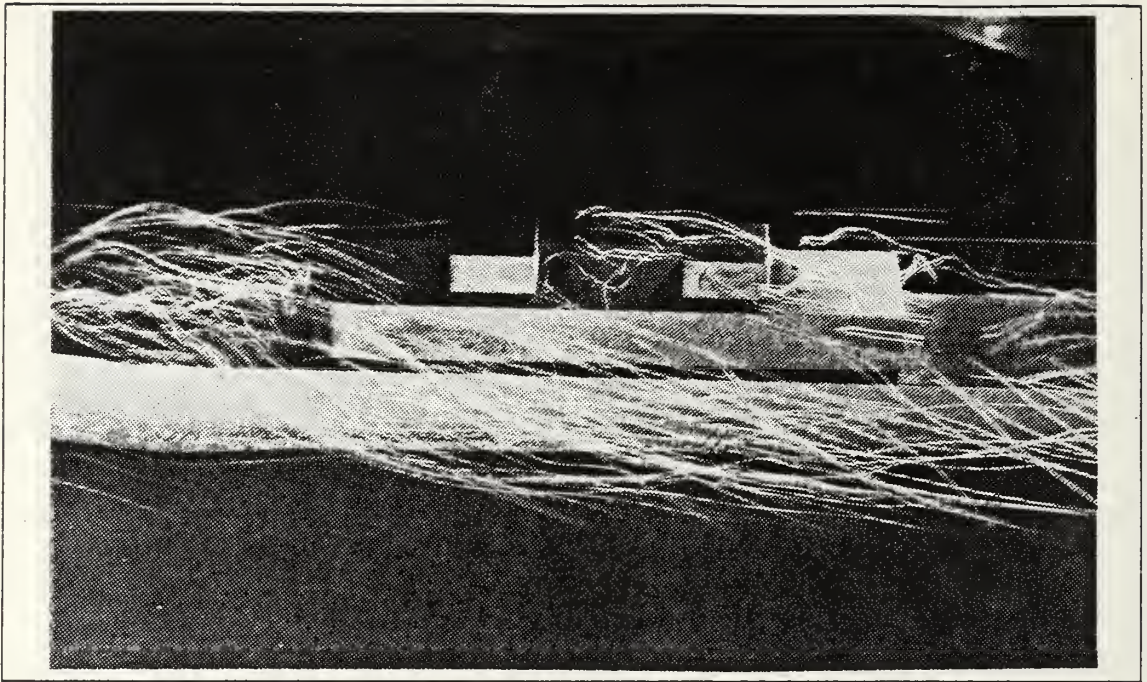
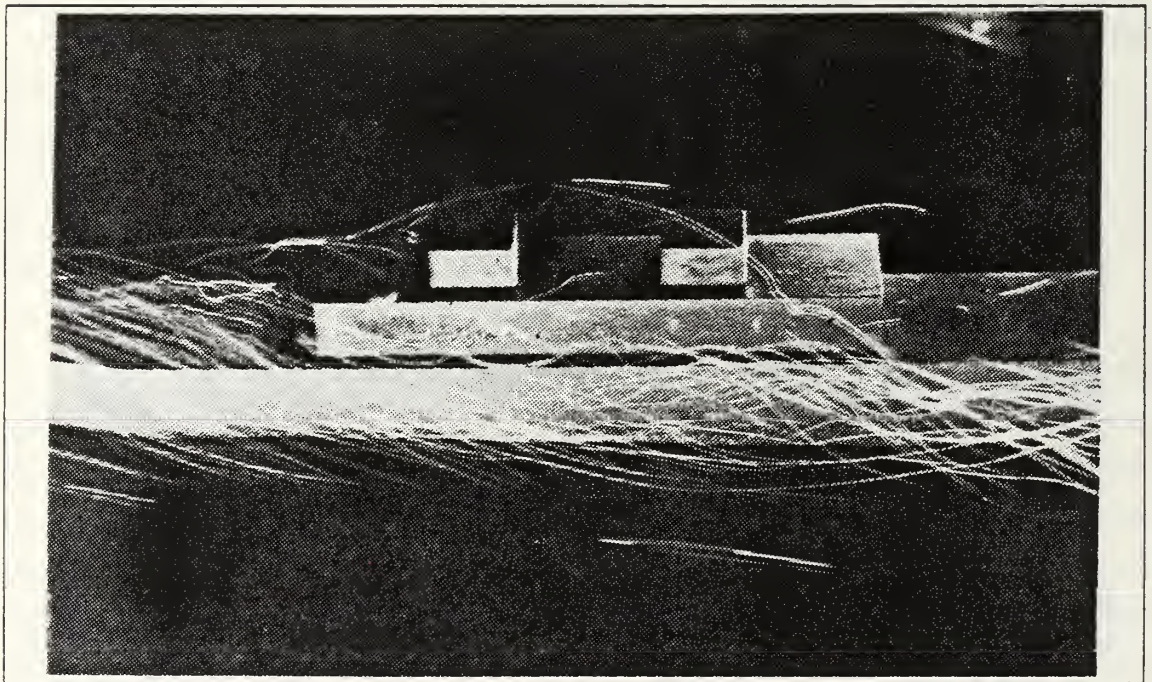Figure 6.14   Nose Up Pitch at 20-Degrees Left Yaw.

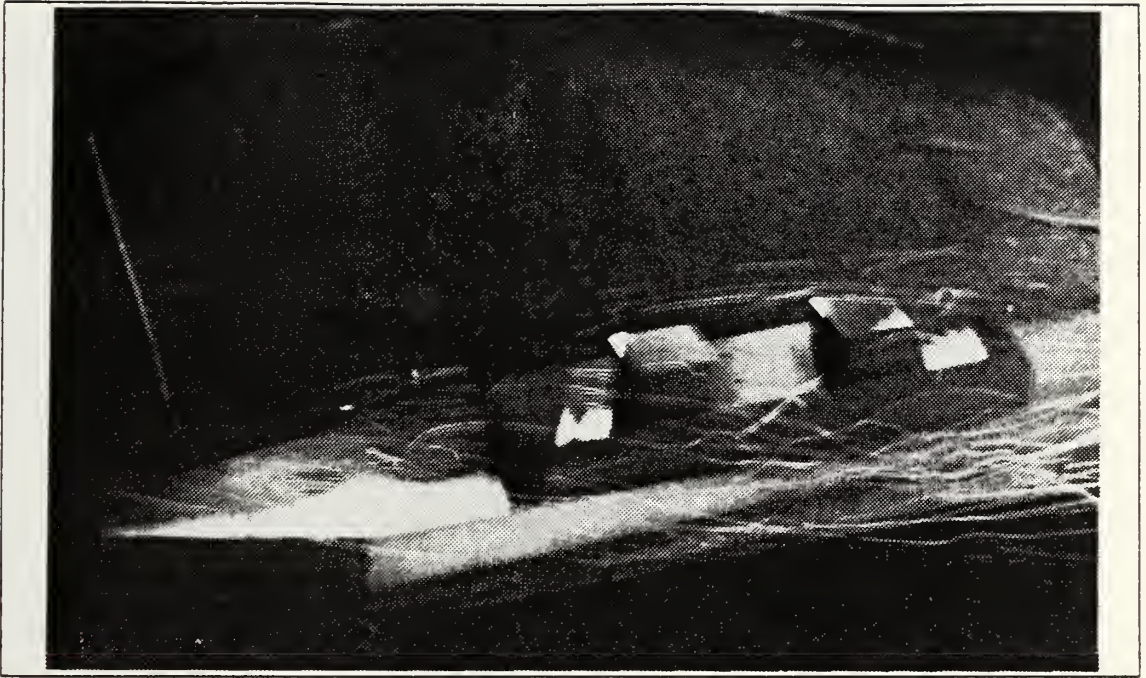Figure 6.15   Nose Down Pitch at 20-Degrees Left Yaw.

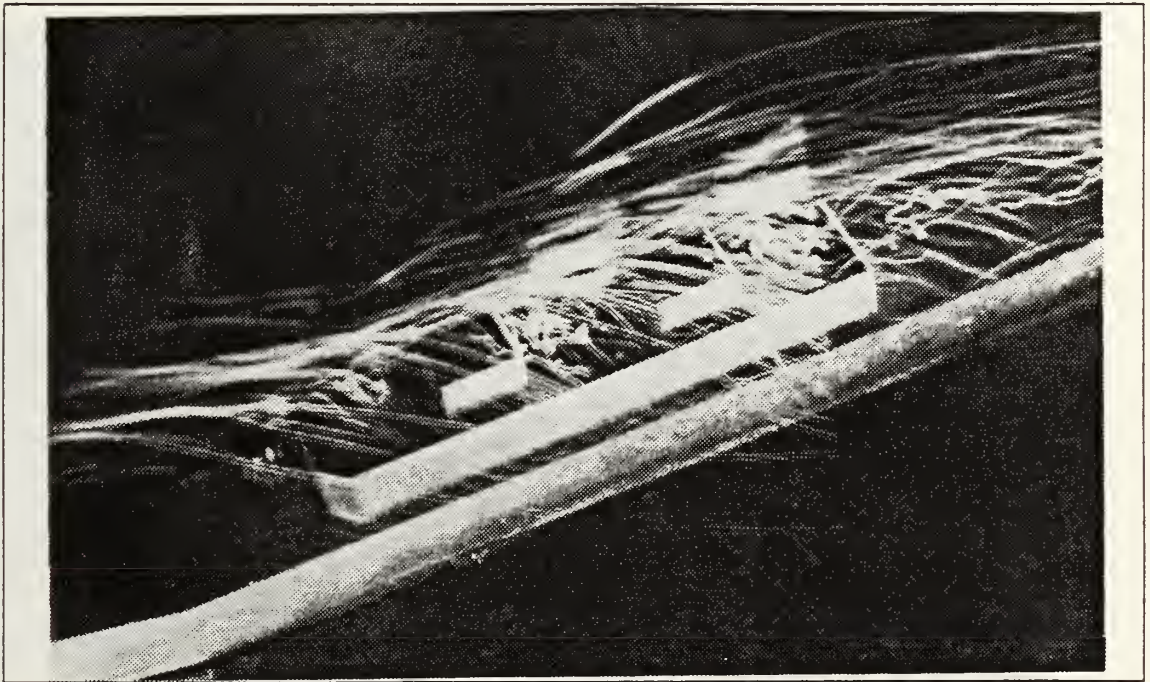Figure 6.16   Oscillating Model at 20-Degrees Left Yaw.

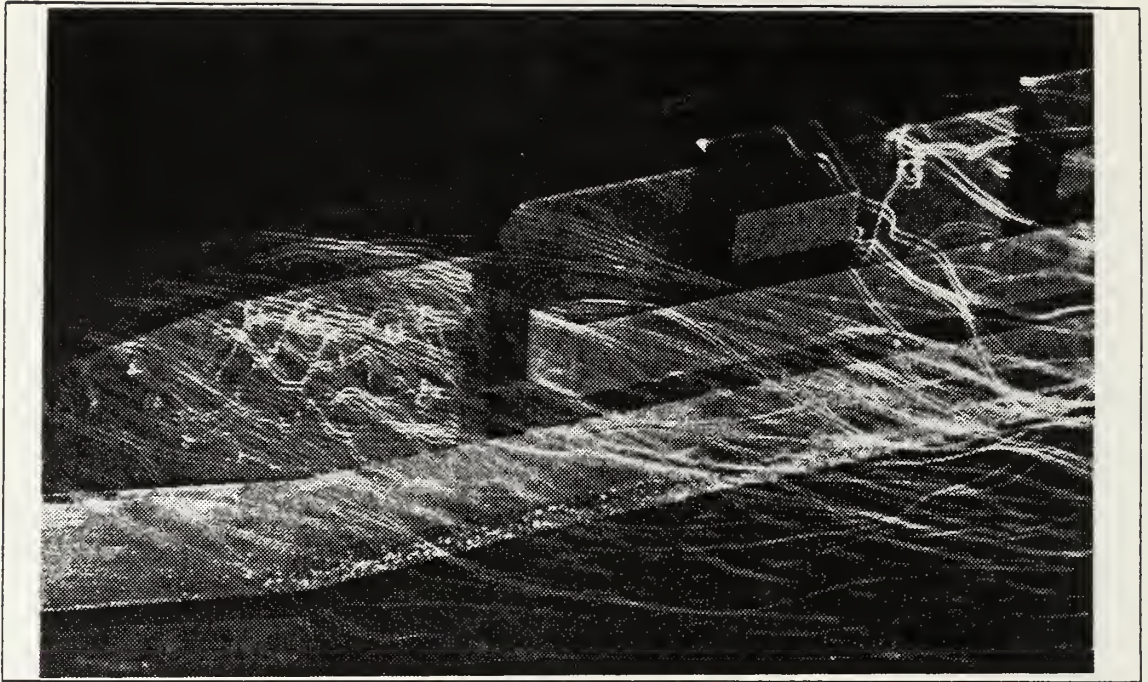Figure 6.17   Zero Pitch and Roll at 35-Degrees Left Yaw.
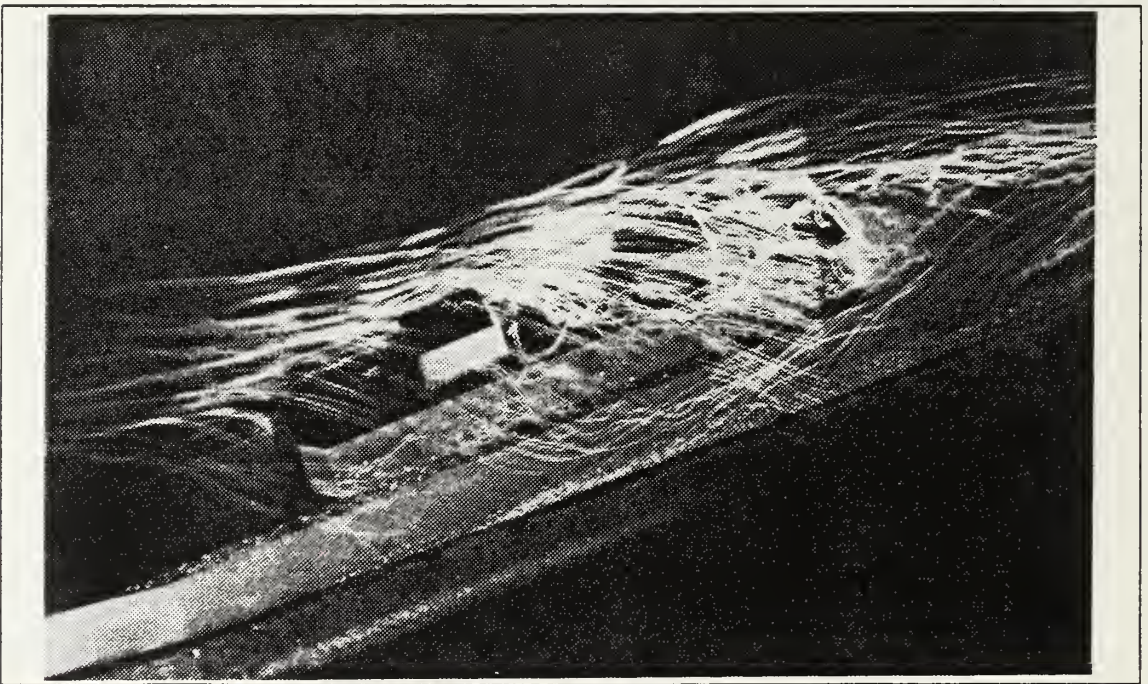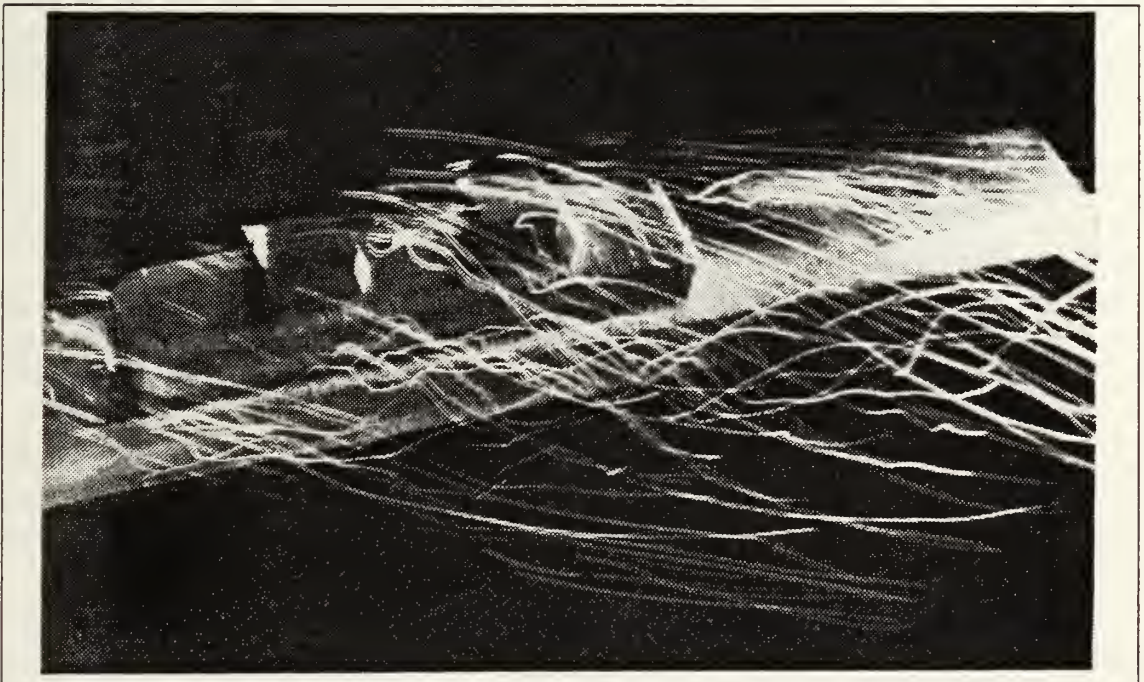
Figure 6.18 Right Roll at 35-Degrees Left Yaw.

Figure 6.19 Nose Down Pitch at 35-Degrees Left Yaw.

Figure 6.20   Nose Up Pitch at 35-Degrees Left Yaw.

Figure 6.21   Oscillating Model at 35-Degrees Left Yaw.

VII. CONCLUSIONS AND RECOMMENDATIONS

This report dealt with the investigation of visualizing the flow field about an oscillating ship model. As a result of this and an earlier study (Ref. 9), the following basic conclusions can be drawn:

(1) The ship motion simulation was a viable first-step approximation to actual ship motion.

(2) The helium bubble flow visualization technique was quite successful for both the static and oscillating cases.

(3) The flow field about both the static model and, to a lesser degree, the oscillating model, was effectly analyzed.

(4) Little determination of coupling effects from the three oscillating modes previously listed was realized. This area requires further flow visualization study combined with accurate data acquisition techniques.

The following recommendations are given for consideraton by those who will continue with the next phases of this project (as discussed in the Introduction):

(1) The use of high-resolution video is strongly recommended for a more exact study of the oscillating mode. In addition to enabling a detailed analysis of the flow field over a wider range of oscillation frequencies, it would provide virtually real-time feedback and bypass the delays involved in developement and printing of photographs.

(2) The fluorescent minituft technique would provide valuable information in the oscillating mode, such as the determination of whether vortex shedding from the model body exists. Future models should incorporate tufting as described in Ref. 9.

(3) Modification to the bubble generator system to possibly increase the bubble output rate would provide the option to photograph at faster shutter speeds. This would make the frequency analysis based on the bubble streaks less complicated.

(4) The author is convinced that the aerosol technique shows enough promise for further modification. One possible avenue, as pointed out in the results section, would be to investigate the effects of increasing the tubing diameter and use higher air pressures to provide a more dense aerosol.

(5) The EIMAC high-voltage arc lamp was responsible for the majority of the high contrast bubble traces. More illumination sources of this type, with an added feature of a geometrically adjustable iris to conform to the model shape, are needed.

(6) Since lighting was one of the biggest obstacles, alternate illumination schemes should be considered. These might include the use of laser sheets, or LED's or optical fibers from within the ship (this would require no adjustment in the static or oscillating case).

(7) The camera shutter should be synchronized to the ship oscillations, which could easily be incorporated with existing hardware. Thus, if recommendation (1.) is unfeasible at this time (due to funding constraints), this would be an alternate method of obtaining a more accurate frequency analysis.

(8) A switch for a second remote to the electronic tachometer would be helpful to facilitate measurement of both modes of motion.

(9) Some analysis of the rolling modes may be obscured due to the motion being in the same plane as the camera angle. Shooting from the ceiling viewing port or even from inside the tunnel may provide some added insight. The latter case would also eliminate problems with reflective glare from the plexiglass.

(10) Flow visualization is only a first step in accurate flow analysis, action is required now to introduce data acquisition methods to achieve more detailed results in the model's areas of interest.

(11) Further study is required into incorporating a more realistic ship motion program into the NPS low-speed wind tunnel.

LIST OF REFERENCES

1. Carico, D., K. E. McMallum, and J.Higman, *Dynamic Interface Flight Test and Simulation Limitations*, paper # 100, pp. 100-1 to 100-19, presented at the Eleventh European Rotorcraft Forum, September 1985.

2. Healey, J. V., "The Prospects for Simulating the Helicopter Ship Interface" *Naval Engineers Journal*, pp. 45-63, March 1987.

3. E.S.D.U. Data Item 74031, Engineering Sciences Data Unit International, Suite 200, Chain Bridge Road, McLean, Virginia 22101.

4. Garratt, J. R., "Review of Drag Coefficients over Oceans and Continents," *Monthly Weather Review*, July 1977, pp. 915, 929.

5. Davenport, A. G., in *Engineering Meteorology*, ed., E. J. Plate, Chapter 12, pp. 527-569, Elsevier Scientific Publishing Company, Amsterdam, Netherlands, 1982.

6. Kent, J. L., *Ships in Rough Water*, Thomas Nelson and Sons Ltd., 1958.

7. Counihan, J., "An Improved Method of Simulation an Atmospheric Boundary Layer in a Wind Tunnel," *Atmospheric Environment*, vol. 3, pp. 197-214, 1969.

8. Arya, S. P., in *Engineering Meteorology*, ed., E. J. Plate, pp.233-267, Elsevier Scientific Publishing Company, Amsterdam, Netherlands, 1982.

9. Bolinger, W. K., *Visualization of the Flow Field Around a Generic Destroyer Model in a Simulated Turbulent Atmospheric Boundary Layer* M.S. Thesis, Naval Postgraduate School, Monterey, California, June 1987.

10. Bearman, P. W., "Vortex Shedding from Oscillating Bluff Bodies," *Annual Review of Fluid Mechanics*, vol. 16, pp. 195-222, 1984.

11. Mueller, T. J., in *Fluid Mechanics Measurements*, ed., R. J. Goldstein, Chapter 7, pp. 307-351, Hemisphere Publishing Corp., 1983.

12. Griffin, O. M., and Ramberg, S. E., "Wind Tunnel Flow Visualization with Liquid Particle Aerosols," pp. 65-73 in *Flow Visualization*, ed., T. Asanuma, Proceedings of the International Symposium on Flow Visualization, 1977, Tokyo, Japan.

13. Blaker, A. E., *Handbook for Scientific Photography*, pp. 1-80, W. H.Freeman and Company, 1977.

INITIAL DISTRIBUTION LIST

11. Mr. R. A. Feik   1
     Aeronautical Division
     Aeronautical Research Laboratories
     506 Lorimer Street
     Fishermans Bend
     Box 4331 P.O.
     Melbourne, Vic. 3001
     Australia